ChemPubSoc Europe
DOI: 10.1002/open.201900133
Open Access ChemistryOPEN Reviews

From Synthesis to Applications: Copper Calcium Titanate (CCTO) and its Magnetic and Photocatalytic Properties

Sara Kawrani,[a, b] Madona Boulos,[b] David Cornu,[a] and Mikhael Bechelany*[a]

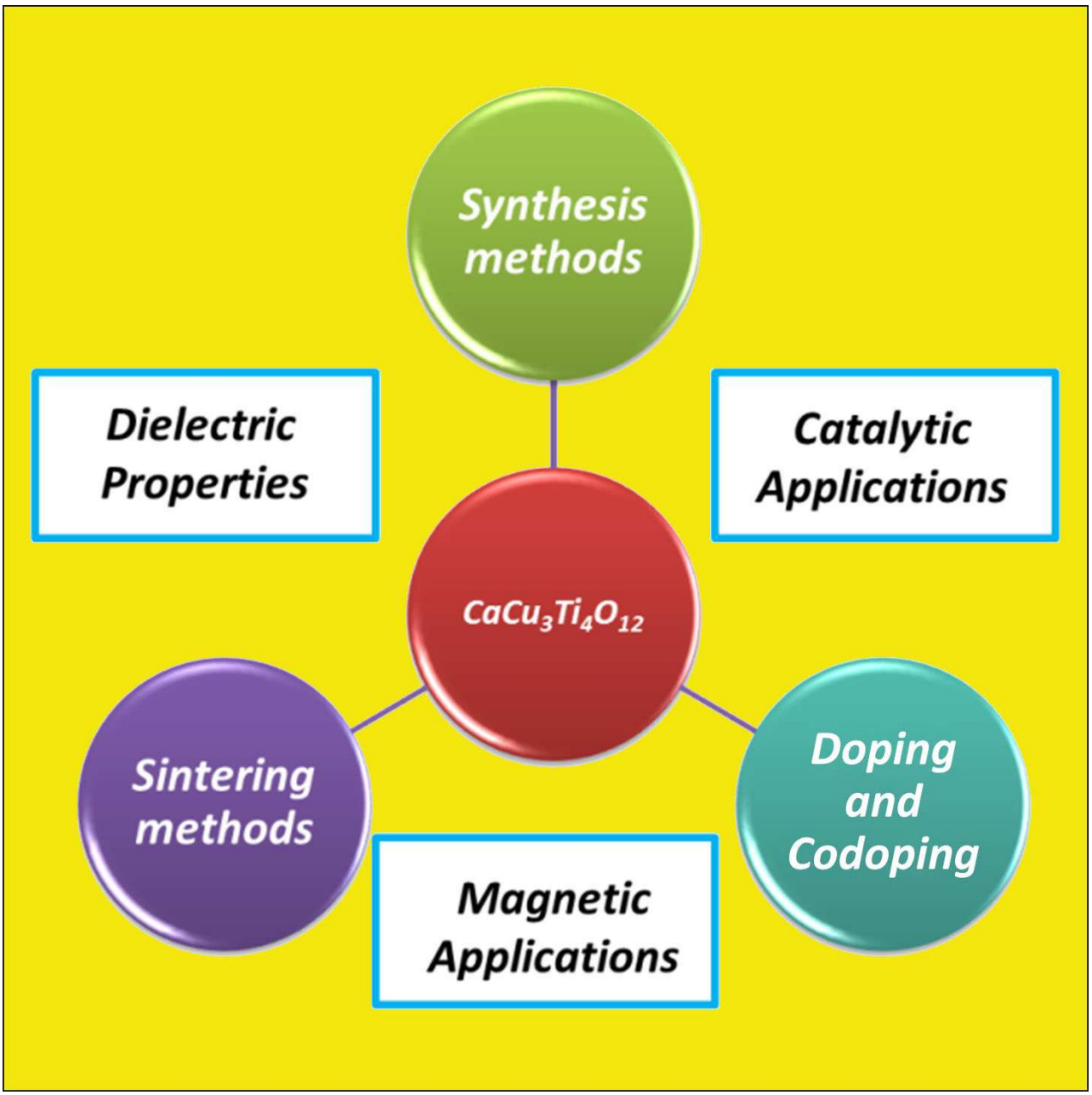

Investigations focusing on electrical energy storage capacitors especially the dielectric ceramic capacitors for high energy storage density are attracting more and more attention in the recent years. Ceramic capacitors possess a faster charge-discharge rate and improved mechanical and thermal properties compared with other energy storage devices such as batteries. The challenge is to obtain ceramic capacitors with outstanding mechanical, thermal and storage properties over large temperature and frequencies ranges. ABO_3 as a type of perovskites showed a strong piezoelectric, dielectric, pyroelectric, and electro-optic properties useful as energy storage and environmental devices. $CaCu_3Ti_4O_{12}$ (CCTO) perovskite with cubic lattice (Im3 symmetry) was discovered to have a colossal dielectric constant (10^4) that is stable over a wide range of frequencies (10 Hz–1 MHz) and temperature independence (100–300 K). The origin of this high dielectric constant is not fully established, specially because it is the same for single crystal and thin films. In this review, the history of CCTO will be introduced. The synthesis and the sintering approaches, the dopant elements used as well as the applications of CCTO will be reported. In addition to dielectrical properties useful to energy storage devices; CCTO could serve as photocatalytic materials with a very good performance in visible light.

1. Introduction

Ferroelectric materials consist of domains with a spontaneous polarization in the absence of an external electric field, and in which this polarization is reversible under the application of an electric field of magnitude less than the dielectric breakdown of the material itself. Spontaneous polarization is the value of charge per unit area on the surface perpendicular to the axis of spontaneous polarization.[1] The magnitude of the net spontaneous polarization possessed by a ferroelectric material starts to decrease while increasing the temperature or the pressure. A phase transition from ferroelectric state to a non-polar paraelectric state took place above a critical temperature T_c (and a critical pressure P_c), called the Curie temperature in which the spontaneous polarization disappears. The structural phase transition from paraelectric to ferroelectric phase is due to the displacement of both cations occupying the A and B sites in the perovskite. This transition may cause a change in dielectric, thermal and other properties of the material.

Ferroelectric materials are divided into four groups; one of these groups is perovskites. A perovskite is a material with the same crystal structure as calcium titanium oxide ($CaTiO_3$). Perovskites have the general formula ABO_3, where A and B are metal cations (ion radius of A is larger than that of B). An ideal structure is cubic with space group symmetry Pm3 m, and it is the simplest example of a structure containing two different cations. Due to the relative sizes of the A and B cations, three types of distortions appear in the simple cubic perovskite structure:

- Distortions of the octahedral units (Jahn-Teller distortion)
- B-cation displacements within the octahedral leading to either a ferroelectric (if all the B atoms move in the same direction) or antiferroelectric (if the B atoms move in opposite directions) structure.
- The relative titling of one octahedral to another. The size of the unit cell increase while reducing the A-site size and no changes in the B-cation environment in such titling.[2] Goldschmidt examined the octahedral titling disordered.[3] In order to determine the stability of perovskite phases, he was based on a formula to define the tolerance factor *t* in the following equation:

$$t = (R_A + R_B)/R_B + R_X) \quad (1)$$

Where R_A, R_B and R_X are the ion radii of the A-site and B-site cations and the X-site anion respectively in an ABX_3 perovskite. The average ionic radius of the ions occupying each site is considered in cases of complex perovskites. The deviation of t values indicates the degree of distortion of a perovskite from the ideal cubic structure.

Barium titanate is a model of ferroelectric materials and belongs to the perovskite group with high dielectric properties. It has been seen that even the crystal structure of calcium titanate ($CaTiO_3$) and barium titanate $BaTiO_3$ is not truly cubic, it is slightly modified.[4] The crystalline phases of barium titanate varied at different temperatures. It is paraelectric at high temperature with a cubic phase, tetragonal and[100] polarized below its Curie temperature ($T_c = 120\,^{\circ}C$), orthorhombic and[110] polarized below 5 °C, and rhombohedral and[111] polarized below −90 °C.

For the miniaturization of electronic devices, high dielectric constant materials are highly useful. Barium titanate and Lead titanate ($PbTiO_3$) perovskites were used widely; they showed different crystalline phases at different temperatures which leads to dielectric properties variation. In addition to that, both $BaTiO_3$ and $PbTiO_3$ showed important dielectric properties useful for capacitor application, but they contain materials which are severally toxic for human body and therefore are non-environment friendly materials,[5] so searching a perovkite with stable properties is important to such applications.

Many researches have been recently investigated the synthesis and characterization of the pseudo-cubic perovskite $CaCu_3Ti_4O_{12}$ (commonly called CCTO), because of its unusual electrical properties. The high dielectric constant 1 KHz for this type of oxides was first reported in 2000 by Subramanian *et al.*[6] Calcium copper titanate was synthetized for the first time using conventional powder-sintering technique. Highly pure starting

[a] S. Kawrani, D. Cornu, M. Bechelany
Institut Européen des Membranes, ENSCM, CNRS, Univ Montpellier, France
E-mail: mikhael.bechelany@umontpellier.fr
[b] S. Kawrani, M. Boulos
Laboratoire de Chimie Physique des matériaux, Université Libanaise, Liban

materials were used (99%) of oxides (CaO, TiO_2 and CuO). The mixed powder was calcined at 900–1000 °C for 8 h, and then the calcined powder was reground and pressed into disks. The disks were sintered in air at 1000–1200 °C.[6]The structure of CCTO (space group *Im3*) can be derived from an ideal cubic perovskite structure ABO_3 by superimposing a body centered ordering of Ca^{2+} and Cu^{2+} that share the A site, and Ti^{4+} is on B site. Due to the different ionic radius between Cu and Ca atoms, a tilting of TiO_6 octahedral planar appears.[7] This distortion forms a square planar oxide environment convenient to Jahn-Teller distorted Cu^{2+}[8] (Figure 1).

CCTO has been found as a material that shows an outstanding dielectric permittivity (up to 10^4) at low frequency and stable at a large frequency scale (10^2 Hz–10^6 Hz). It has been noticed that this giant dielectric permittivity is temperature independent over a wide temperature range between 100 and 600 K[9] which makes this oxide very attractive for technological applications. Despite the high permittivity, CCTO loss tangent still high and constitute an obstacle for commercial applications.[10,11] The origin of this important permittivity is not fully understood and many hypotheses based on intrinsic and extrinsic properties were suggested. Subramanian *et al.* suggested an intrinsic origin for this high permittivity explained by a ferroelectric relaxation that affects the rearrangement of Ti^{4+} ions,[6] Sinclair *et al.*[7,12–14] showed that the high permittivity is due to an internal barrier layer capacitor and not to an intrinsic feature of the bulk crystal structure. They demonstrated that CCTO ceramics are formed from semiconducting grains separated by insulating grains boundaries and they suggested an electrical model that consists of two parallel capacitance-

Sara Kawrani was born in November 1993 in Lebanon. She received her BS degree in Chemistry from department of chemistry, faculty of sciences Hadath-Lebanese University in 2014. Then she obtained Maters II degree in Physical Chemistry of materials from faculty of science Fanar-Lebanese Univerity. She continued pursuing her phd degree at University of Montpellier at European Institute of Membranes (IEM) under the supervision of Pr. David Cornu and Dr. Mikhael Bechelany in a collaboration work with Lebanese University- faculty of sciences Fanar under the supervision of Dr. Madona Boulos. She is interested in synthesis of perovskite materials and exploring their behaviors for renewable energy and photocatalytic application.

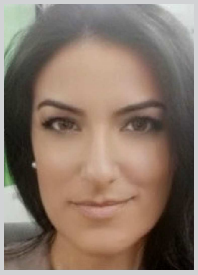

Dr Madona BOULOS received her master degree in Materials and Analytical chemistry from the University Strasbourg 1 (France) in 2002, and her Ph.D. in Materials sciences from the University Toulouse III (France) in 2005 (Centre InterUniversitaire de Recherches et d'Ingenerie des Matériaux – CIRIMAT) under the supervison of Pr. Bernard Durand and Dr. Sophie Guillemet Fritsch. Her main achievement was the synthesis of titanates powders by soft chemistry methods (hydrothermal and coprecipitation) showing colossal dielectric properties. Since 2006 she is an assisstant Professor at the Lebanese University and a member in the "Laboratoire de Chimie Physique des Matériaux" (LCPM) where she works on the synthesis of different oxide powders using the mechanical alloying method and their physico-chemical characterizations.

Professor David CORNU received his master degree in materials chemistry from the University Lyon 1 (France) in 1995, and his Ph.D. from the same university in 1998 (Laboratoire des Multimatériaux et Interfaces (LMI), Pr. H. Mongeot and CNRS senior researcher Dr. B. Bonnetot). After post-doctoral researches in the lab of Prof. M. F. Lappert (University of Sussex, Brighton UK), he obtained a position of Assistant Professor at the University Lyon 1 (LMI, Prof. P. Miele) in 1999. His research interests were boron chemistry, polymer-derived ceramics and nanowires/nanotubes. In 2008, he accepted a Professor position at the Ecole Nationale Supérieure de Chimie de Montpellier (ENSCM), a French elite graduate school, and within the Institut Européen des Membranes (IEM). He is director of industrial relations and technology transfer office of ENSCM since 2012. His research activities are mainly focused on electrospinning and inorganic nanomaterials as building blocks to construct porous materials/membranes for biotechnologies, health and energy applications. He is co-authored of more than 120 publications (g.scholar h = 31) and co-deposited 10 patents.

Mikhael BECHELANY (born in March 1979) obtained his PhD in Materials Chemistry from the University of Lyon (France) in 2006. His PhD work was devoted to the synthesis and characterization of silicon and boron based 1D nanostructures (nanotubes, nanowires and nanocables).
Then, he worked as a post-doc at EMPA (Switzerland). His research included the fabrication of nanomaterials (nanoparticles and nanowires), their organization and their nanomanipulation for applications in different field such as photovoltaic, robotic, chemical and bio-sensing.
In 2010, he became a Scientist at CNRS. His current research interest in the European Institute of Membranes (UMR CNRS 5635) in Montpellier (France) focuses on novel synthesis methods for metals and ceramics nanomaterials like Atomic Layer Deposition (ALD), electrospinning and/or on the nanostructuring using nanospheres lithography, Graphene and Graphene like materials. His research efforts include the design of nanostructured membranes for health, environmental and renewable energy applications.

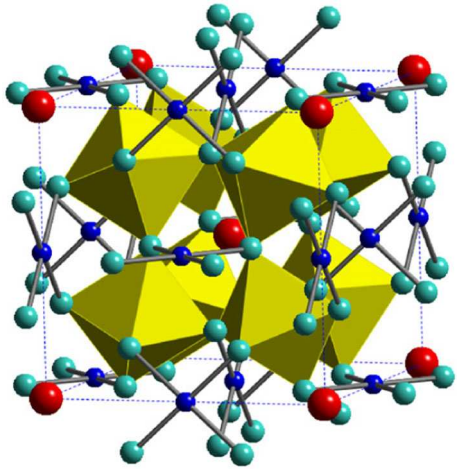

Figure 1. Structure of the cubic pseudo-perovskite (Im3) $CaCu_3Ti_4O_{12}$ with TiO_6, Cu in square planar coordination (small black spheres) about O (small light grey spheres) and Ca at the origin and cube center (medium size grey spheres). Reprinted with permission from (Subramanian et al., 2009). Copyright 2009 Elsevier.[9]

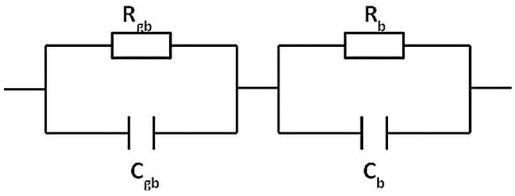

Figure 2. Simplified equivalent circuit consisting of two parallel RC elements connected in series. Updated from reference.[15]

resistance (RC) elements, R_gC_g and $R_{gb}C_{gb}$ representing semiconducting grains and insulating grains bhoundaries respectively, both connected in series[7] (Figure 2). It is now fully accepted that the origin of the exceptional electrical properties of CCTO ceramics are due to an internal barrier layer capacitance (IBLC) origin.

Basing on the experimental results, it has been possible to use CCTO for fabricating an efficient energy storage device (EDS), and can be used for the evolution of solid state capacitors of class II type. In addition to that, CCTO is a wide gap n-type semiconductor material and can be used for high temperature electronics, basing on studies of the resistivity at high temperature.[16]

However decreasing dielectric loss with maintaining a high dielectric constant is the challenge. Many investigations have been done to understand the origin of these dielectric properties and their relation with CCTO crystal structure.

Several reviews focusing on different perovskite materials and their dielectric properties such as barium titanate ($BaTiO_3$)[17] and Lead titanate ($PbTiO_3$)[18] have been reported recently. In 2016, Ahmadipour *et al.* reported CCTO ceramics and films fabrication, factors influencing its dielectric properties and its sensing applications.[19] Here, an overview on the influence of experimental conditions such as synthesis method, sintering approaches and doping elements on the structures and dielectric properties of CCTO will be provided. The new trend in this field (since 2016) will be mainly discussed. This review will focus, in addition to electrical properties, on the photocatalytic and the magnetic applications of CCTO, two interesting properties that have not been reviewed before.

This review is composed from five sections. In first section, the synthesis methods are discussed. The following section will report the sintering approaches and their influence on dielectric properties. In the third part, different doping elements as well as their influence on the morphology and the dielectric properties of CCTO will be discussed. Finally the new properties of CCTO such as magnetic and photocatalytic properties will be reviewed.

2. Synthesis Methods

In this section the synthesis methods used to design calcium copper titanate such as solid state route (solid-solid, mechanosynthesis method), wet chemistry method or soft chemistry (sol-gel, coprecipitation, hydrothermal method), microwave synthesis and combustion synthesis techniques will be reported.

2.1. Solid State Route

Solid state route is the first method used to prepare oxide. It is a mixing of solid starting materials. Since those solids do not diffuse in each other at room temperature to form the final compound, an additional step of heating at high temperature is necessary. Solid-state route is divided into two groups, solid-solid by mixing manually the powders in an agate mortar and mechanosynthesis method by using a ball mill machine to mix the precursors.

The CCTO, for dielectric applications, is very largely prepared by the "solid-solid" route. This method consists in making an intimate mixture of oxide powders or precursors of oxides (carbonates, hydroxides or nitrates) of calcium, copper and titanium. Subramanian *et al.*[6] used oxides and carbonates precursors which they calcined at 1000 °C. Unfortunately in order to obtain at the end a proper, homogeneous and single phase material, several steps of grinding and calcination at high temperature are required. This is the reason why finding new methods that are rapid and environmentally safe was developed later.

The mechanochemical synthetic route (Figure 3) is a simple and rapid method that allows the direct synthesis of the single phase oxides at low temperatures. One of the most important advantages of this technique is that the starting materials can react together by a simple diffusion mechanism at room temperature. The diffusion mechanism is due to the mechanical stress applied on the precursors during the synthesis. In addition the grains size is reduced during this process.[20]

The chemical reaction during the solid-solid and a mechanochemical reaction method for the synthesis of CCTO is shown in equation **2**:

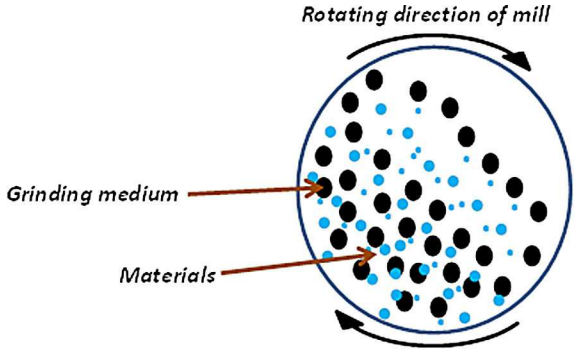

Figure 3. Schematic diagram of a ball mill.

$$CaCO_3 + 3CuO + 4TiO_2 \rightarrow CaCu_3Ti_4O_{12} + CO_2 \uparrow \quad (2)$$

Recently mechanical alloying method is used to prepare CCTO by mixing $CaCO_3$, TiO_2 and CuO with or without solvent, followed by a calcination step to synthetize single pure phase of CCTO.[14,21–23]

Thirpathy *et al.*[24] mixed a stoichiometric amount of $CaCO_3$, TiO_2 and CuO into acetone (as a dispersant agent) using a ball mill in a sealed plastic bottle with zirconium beads. Powders were calcined at different temperatures from 900 °C to 1050 °C for 10 h. Pellets were then sintered at 1100 °C for 8 h. XRD patterns (Figure 4a) showed that the pure phase of CCTO is

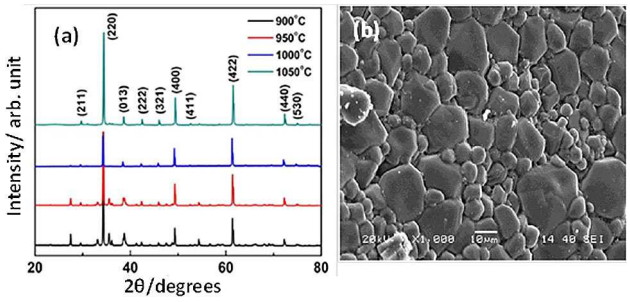

Figure 4. (a) X-ray diffraction patterns of CCTO powder calcined at different temperature and (b) SEM micrograph of CCTO pellet. Reprinted with permission from (triphathy et al. 2016). Copyright 2016 Creative Commons CC.[24]

given at 1050 °C of calcination. As seen in SEM images, (Figure 4b) large grains are surrounded by small ones at the junction for sintered pellets.

Figure 5 (a) showed the frequency dependence of dielectric constant as the function of temperature (30 °C–310 °C). The permittivity (ε′) value decreases with increasing the frequency, and at some point, ε′ increases while increasing temperature. This behavior could be related to the accumulation of charge on interface. Figure 5 (b) showed that the dielectric loss is stable at high frequencies and increases at low frequencies and high temperature, this phenomenon is might due to the increase of conductivity with temperature.

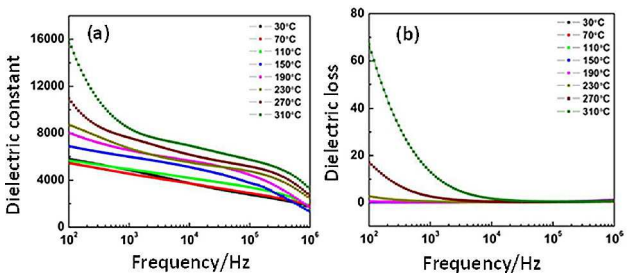

Figure 5. (a) Frequency dependence of dielectric constant of CCTO pellet at different temperatures and (b) Frequency dependence of dielectric loss of CCTO pellet at different temperatures. Reprinted with permission from (triphathy et al. 2016). Copyright 2016 Creative Commons CC.[24]

Even if these methods are easy and simple to perform, they suffer from the need of repetitive grinding and the use of a very high temperature for calcination.

2.2. Wet Synthesis or Soft Chemistry

Over the past thirty years, new methods improperly called "chemical" have been proposed to develop ceramic oxide powders of higher quality than those obtained by the solid route. Greater purity, better granulometric characteristics and higher reactivity, were reported thus leading to significantly lower sintering temperatures. Among these methods, there are two main categories: (i) wet synthesis methods under normal atmospheric pressure such as sol-gel and coprecipitation methods and (ii) hydrothermal methods.

2.2.1. Sol-Gel Method

Sol-gel method is one of the well-established synthetic approaches to prepare novel metal oxides nanoparticles. This method has potential control over the textural and surface properties of the materials. Sol–gel method mainly undergoes in few steps to deliver the final metal oxide protocols and those are hydrolysis, condensation, and drying process. The control of kinetics of hydrolysis and condensation of the titanium ions is sought in this type of synthesis. The basic idea is to slow down the formation of Ti-O-Ti sequences to favor the formation of Ti-O-Ca and Ti-O-Cu sequences which prefigure the crystalline structure of calcium cupper titanate instead of TiO_2. The slowing down of the Ti-O-Ti linkages is caused by a low water supply or by titanium ion fixation of groups such as acetate. The kinetics can also be slowed down by simply lowering the temperature.

The precursors used in this method are metal alkoxide, metal citrate or nitrate. Micrometers particles are distributed by mechanical mixing in a liquid, to form colloidal or sol solution with adjusted pH (Figure 6). Some difficulties are associated with the key steps of this method such as hydrolysis, condensation and drying, which affect directly the morphology of the material.

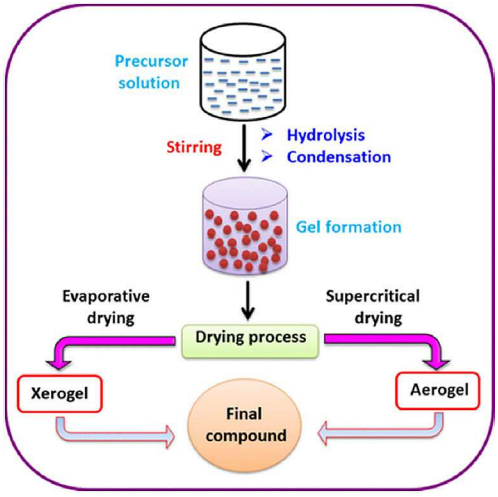

Figure 6. The Reaction Pathway for the Production of Metal Oxide Nanostructures in the Sol–Gel Method. Reprinted with permission from (Rao et al. 2017). Copyright 2017 Elsevier.[25]

Mao *et al.*[26] have synthesized CCTO using calcium nitrate $Ca(NO_3)_2 \cdot 4H_2O$, copper nitrate $Cu(NO_3)_2 \cdot 3H_2O$, titanium isopropoxide ($Ti(C_3H_9O)_4$, citric acid ($C_6H_8O_7$) and ethylene glycol ($C_2H_6O_2$) as starting materials. A stoichiometric amount of Ca $(NO_3)_2 \cdot 4H_2O$ and $Cu(NO_3)_2 \cdot 3H_2O$ were dissolved in ethanol and the pH was adjusted by the addition of citric acid to form solution (A). Solution (B) is formed by mixing $(Ti(C_3H_9O)_4$ and ethanol for 1 h, then solutions (A) and (B) were mixed together with ethylene glycol at room temperature for 1 h to obtain a clean and transparent sol solution. In order to obtain a viscous blue gel, this solution was heated at 90 °C in a drying oven, then heated to 120 °C and kept for 12 h in the drying oven to gain fluffy precursor powders. The precursor powders labeled CCTO from 1 to 6 were calcined at 650 °C, 700 °C, 750 °C, 800 °C, 850 °C and 900 °C for 3 h respectively then pressed to form pellets and sintered at 1050 °C/10 h.

The XRD patterns for the obtained powders and ceramics are shown in (Figure 7). It is clear that CCTO is formed and well crystallized. However traces of CuO and TiO_2 phases are observed in powders calcined at 900 °C.

From SEM images they concluded that the grain size distribution depends on the calcination. CCTO labeled 1, 2 and 3 ceramics had homogeneous microstructures, for CCTO labeled

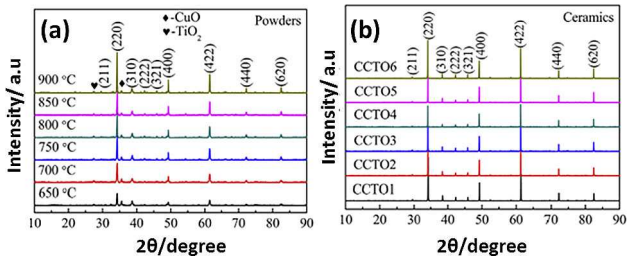

Figure 7. XRD patterns of the CCTO powders calcined at different temperature (a) and the sintered CCTO ceramics at 1050 °C for 10 h (b). Reprinted with permission from (Mao et al., 2019). Copyright 2019 Elsevier.[26]

from 4 to 6 ceramics large grains are obtained. This could be attributed to the presence of small grains absorbed by large grains. Grain boundaries of CCTO 5–6 ceramics are heterogeneous and large grains are formed.

At low frequency (10^2 Hz) the permittivity and the dielectric loss increase with increasing calcination temperature, and the increasing of the grain size. Thus, the CCTO6 had the highest value for permittivity and tanδ. At medium frequency (10^3–10^5 Hz) it has been observed that CCTO5 exhibit the lowest value of tanδ (0.091).

Compared with the solid route where the homogeneity scale is rarely better than 0.5 μm, the sol gel method showed considerable advantages, including excellent chemical stoichiometry, compositional homogeneity, and lower crystallization temperature.

2.2.2. Co-Precipitation

Co-precipiation is one of the most convenient techniques for the preparation of nanomaterials with a narrow size distribution. The co-precipitation technique does not require costly equipment, stringent reactions or complex procedures. This method is based on mixing stoichiometric amounts of soluble salts of metals to form a precipitate of hydroxides, oxalates, or citrates and then the mixture is filtered, dried and heated to form the final product.

Zhu *et al.*[27] used co- precipitation method to synthetize CCTO powders. They started by dissolving 0.2 mole of oxalic acid in ethanol, the pH of the obtained solution was adjusted to 2.5–3 using ammonia. At this point, 0.1 mole of $Ti(OCH_4H_9)_4$ were added. On the other hand a stoichiometric amount of calcium nitrate (0.025 moles) and copper nitrate (0.075 moles) were dissolved in distilled water. After few minutes, the metal nitrates solution and the oxalic solution were mixed and kept overnight to complete the reaction. The precipitate was filtered, dried then calcined. Pellets were pressed and sintered by spark plasma sintering at 1000 °C for 2 h.

Figure 8a shows the XRD patterns of the powders obtained at different calcination temperatures. They confirm the formation of pure CCTO at 700 °C calcination temperature.

SEM image of the obtained ceramic (Figure 8b) showed a dense microstructure with an average grain size between 2 and 5 μm. The sintered pellets showed a high dielectric constant $> 10^4$, that increases with frequency from 1 KHz to 1 MHz due to IBLC model effect.

Using coprecipitation method will help to obtain CCTO at low calcination temperature.

2.3. Microwave Synthesis

Microwave energy was originally applied for heating food. Recently it has been used to accelerate chemical synthesis. Thus, the microwave energy replaces the calcination step to obtain the pure phase of CCTO powders. The heating effect utilized in microwave assisted synthesis is mainly due to

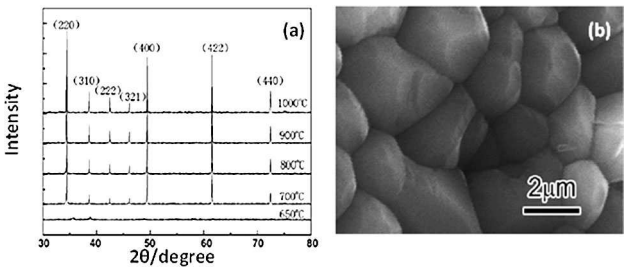

Figure 8. a) XRD patterns of CCTO calcined in air at various temperature,(b) the SEM photograph of CCTO ceramic bulk. Reprinted with permission from (Zhu et al., 2009). Copyright 2009 Elsevier.[27]

dielectric polarization. This method is based on the emission of a radiation into a solution. If the solution contains charged particles, this particle will move under the influence of a field and produce an oscillating electric current. If the particles in the solution are not charged, the electric field component will cause them to align the dipole moments and this is the dielectric heating. To use the microwave heating techniques, the compound must contain at least one molecule that can absorb the radiation or must be surrounded by an absorbent molecule to absorb microwave radiations.

Kumar *et al.*[28] used the microwave flash combustion technique to synthetize CCTO, involving microwave irradiation on aqueous solution containing $Ca(NO_3)_2 \cdot 4H_2O$, $Cu(NO_3)_2 \cdot 4H_2O$, $TiO(NO_3)_2$ as an oxidizer and urea (CH_4N_2O) as a fuel. They prepared an aqueous solution of two precursors $Ca(NO_3)_2.4H_2O$ and $Cu(NO_3)_2.4H_2O$ separately, then they mixed these solutions with an stoichiometric amount of urea fuel and oxidizer agent ($TiO(NO_3)_2$). At the end, they obtained a blue gel. This gel is kept in an alumina crucible and put into a microwave costumed oven operating at 2.45 GHz and 1.1 KW power. The combustion takes around 30s to be completed. It is accomplished by a flash of light followed by discharge of gaseous mixture (O_2, N_2, H_2O) and a porous dark-brown residue is obtained. This residue was crushed then calcined at 800 °C and 900 °C for 5 h to obtain CCTO. XRD patterns (Figure 9a) showed that the pure phase of CCTO is obtained after calcination at 900 °C/5 h.

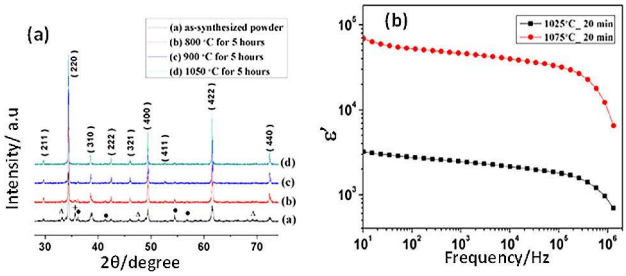

Figure 9. (a) XRD patterns of CCTO powder samples: (a) as-synthesized, (b) calcinated at 800 °C for 5 h, (c) calcinated at 900 °C for 5 h, and (d) sintered pellet at 1050 °C for 5 h. The symbols Δ, +, and • correspond to the trace of secondary phases $CaTiO_3$, CuO, and TiO_2, respectively, (b) Frequency dependence of the dielectric constant and tan δ of sintered CCTO samples sintered at 1050 °C for 5 h. The inset shows the variation of the real part of the impedance with frequency. Reprinted with permission from ref. [28]. Copyright © 2015 American Chemical Society

Dielectric properties (Figure 9b) were studied on CCTO pellet (sintered in air with conventional method at 1050 °C/5 h) and showed that at low frequencies dielectric constant increases, that maybe due to the ceramic-electrode interface effect or to a relaxation dipole at the grain boundaries. However higher dielectric constant and dielectric loss appear at high frequency (0.5–8 MHz). This value of dielectric loss is maybe due to that at high frequency just the response of grains is considered and there is charge carriers generated in grains during sintering by reduction of Cu^{2+} to Cu^{+} and by oxygen loss.

Despite that this approach is very elegant, the final compound cannot be formed after heating into a microwave and a second step of calcination is always needed.

2.4. Combustion Synthesis Technique

By this method, single homogenous nanopowders and single-phase material can be produced; ceramics, catalysis composites alloys and nanomaterials are synthetized and proceeded. A reaction is maintained between a fuel and an oxidant present in the precursor solution. Oxidant are the nitrates of different metals and the fuel generally are citric acid, urea, ethyl glycol or it can be added with some chelating agents such as acetic acid, to form complexes with the metal ions present in the precursor solution. The dehydration of this complex produces a viscous gel, that after self-heating produce a huge quantity of gazes which leads to the formation of pores. The final step is the calcination at high temperature of this gel to have a final product.

Patra *et al.*[29] used an appropriate amount of $TiO(NO_3)_2$, $CaCO_3$, CuO, citric acid monohydrate and ammonium nitrate. The pH of the solution was adjusted using NH_4OH, the solution was kept on a hot plate at 80–90 °C. A viscous gel is developed due to the dehydration of the mixed solution during heating. This gel self-ignites resulted from heating is followed by swelling of the gel. A voluminous black precipitate was obtained from this ignition, and then calcined at 800 °C to obtain pure CCTO phase.

Lopera *et al.*[30] used sol-gel method associated with auto-combustion to synthetize Sm-doped $CaCu_3Ti_4O_{12}$. They used (Cu $(NO_3)_2$), $(Ca(NO_3)_2)$ Ti-isopropoxide ($Ti[OCH(CH_3)_2]_4$,) Samarium nitrate ($Sm(NO_3)_2$), and acid citric ($C_6H_8O_7H_2O$). In order to have $Ca_{1-x}Sm_xCu_3Ti_4O_{12}$ (for $x=0$, $x=0.2$,$x=0.3$), starting materials were mixed in distilled water solution then heated on a hot plate magnetic stirrer at 70 °C until the auto-combustion is achieved. Precursor powders are sintered at 1050 °C/10 h. XRD patterns (Figure 10) showed that a pure phase of CCTO is formed with almost the same lattice parameter 7.392 Ä, 7.394 Ä and 7.395 Ä for CCTO ($x=0$), CCTO2 ($x=0.2$) and CCTO3($x=0.3$) respectively. SEM images showed that grain growth was inhibited after doping by Sm^{3+}, and the permittivity at 100 kHz decrease from 15.747 for undoped CCTO to 4126 for CCTO3.

Autocombustion method is a rapid process with low-cost and low-temperature. There is a possibility to have multi-component oxides with single phase and high surface area. It is

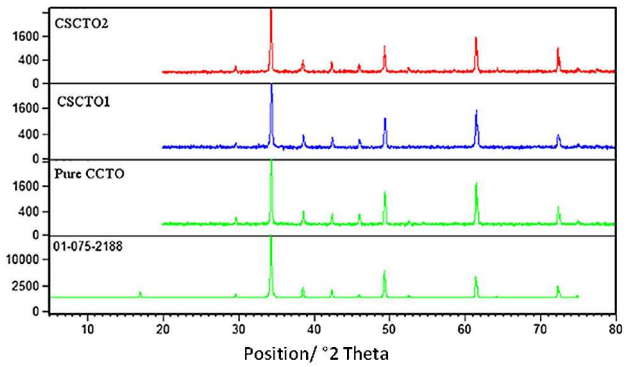

Figure 10. X-ray diffraction patterns for $Ca_{1-x}Sm_xCu_3Ti_4O_{12}$ the system CSCTO2 (x = 0.2), CSCTO1 (x = 0.3), and CCTO (x = 0.0). Reprinted with permission from (Lopera et al., 2014). Copyright 2014 Elsevier.[30]

an exothermic reaction that makes the product almost instantaneously. The disadvantages of this process are the possibility of contamination with carbonaceous residue and the poor control of morphology.

2.5. Hydrothermal Method

Hydrothermal method is used in order to synthetize nanosized ceramics. To carry out the reaction under high temperature and pressure, precursors are placed into an autoclave filled with water.

Classically to synthesize CCTO by hydrothermal method [$Ti(OC_3H_7)_4$], $CaCO_3$, $Cu(NO_3)_2 \cdot 2.5\ H_2O$ and potassium hydroxide (KOH) are used as starting materials. In deionized water, an appropriate amount of titanium isopropoxide and calcium carbonate was dissolved, the same for copper nitrates, then the two solutions were mixed together with 50 mL from KOH (mineralizer). An amorphous precipitate of $Ti(OH)_2$, $Ca(OH)_2$ and $Cu(OH)_2$ is formed. In order to avoid the formation of calcium carbonate as second phase, nitrogen gas was constantly bubbled to the system. The mixture is transferred to a Teflon autoclave.

Masigboon *et al.*[31] synthetized $CaCu_3Ti_4O_{12}$ using the hydrothermal method. In aqueous medium, precursors Ca $(NO_3)_2 \cdot 4H_2O$, $Cu(NO_3)_2 \cdot 3H_2O$, $Ti(OC_3H_7)_4$ and freshly extracted egg white (ovalbumin) were mixed. Egg white protein was used due to his gelling, foaming and emulsifying characteristics. It was no need to pH adjustment with this process. Mixed solutions were treated hydrothermally in autoclave at 150 °C and 200 °C for 8 h. They dry the precursor at 70 °C–80 °C then it was calcined at 800 °C, 900 °C and 1000 °C/8 h.

XRD patterns (Figure 11) showed that the pure phase of CCTO appears after 800 °C of calcination with second phases $CaTiO_3$, TiO_2 and CuO. $CaTiO_3$ appears when there is non-stoichiometric amount of Titanium and calcium. As seen in TEM images (Figure 12), CCTO had a nanocrystalline structure, in

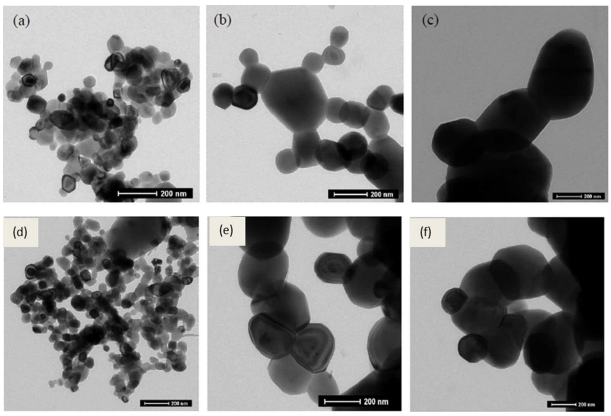

Figure 12. TEM images of CCTO powders, which prepared by hydrothermal process at 150 °C/8 h calcined in air for 8 h at (a) 800, (b) 900 and (c) 1000 °C, and at 200 °C/8 h calcined in air for 8 h at (d) 800, (e) 900 and (f) 1000 °C, respectively. Reprinted with permission from (Masingboon et al. 2017). Copyright 2017 Creative Commons CC.[31]

which grain size increases with calcination's temperature. They conclude that with hydrothermal method, CCTO powders can be produced in order to study their dielectric properties.

To prepare calcium copper titanate, different synthesis methods are used. The aim of using these methods (apart from the solid state route) was to obtain the final compound at lower calcination temperature and with a homogeneous microstructure in order to maintain a high permittivity and a low dielectric loss. In Table 1, some selected examples for these different

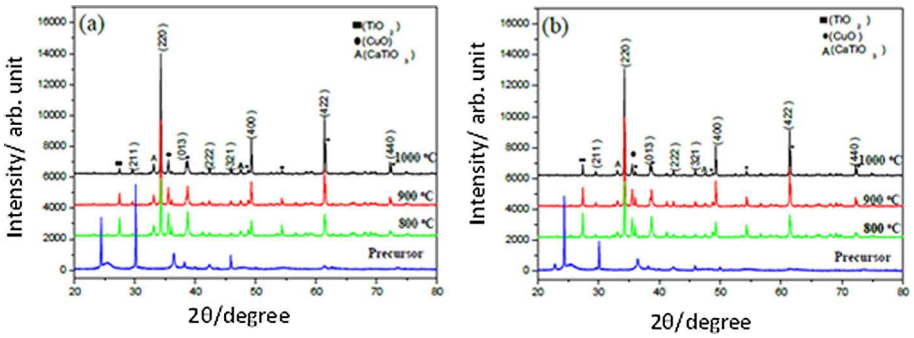

Figure 11. XRD patterns of CCTO base-powders prepared by hydrothermal process at (a) 150 °C/8 h and (b) 200 °C/8 h, respectively. All powders calcined in air for 8 h at 800, 900 and 1000 °C. Reprinted with permission from (Masingboon et al. 2017). Copyright 2017 Creative Commons CC.[31]

Table 1. Resumed comparison between synthesis method and their influence on dielectric properties permittivity (ε'), and dielectric loss (tan δ).

Synthesis Method	Precursors	ε'	tan δ	References
Solid-solid	CaO,CuO and TiO_2	10,286	0.067	[6]
Mechanosynthesis	$CaCO_3$, CuO, TiO_2	~5000	0.14	[21]
Sol-gel	$Ca(NO_3)_2 \cdot 4H_2O$, Cu $(NO_3)_2 \cdot 3H_2O$, Ti $(C_3H_9O)_4$, $C_2H_6O_2$, $C_6H_8O_7$	$3*10^4$	0.091	[25]
Microwave synthesis	$Ca(NO_3)_2 \cdot 4H_2O$, Cu $(NO_3)_2 \cdot 4H_2O$, TiO $(NO_3)_2$, CH_4N_2O	53,300	0.2	[27]
Autocombustion	$Ca(NO_3)_2$, $Cu(NO_3)_2$, Ti $[OCH(CH_3)_2]_4$, $C_6H_8O_7H_2O$	15,474	-	[29]
Coprecipitation	$H_2C_2O_4 \cdot H_2O$, Ca $(NO_3)_2 \cdot 4H_2O$, $Cu(NO_3)_2 \cdot 3H_2O$, Ti $(OC_4H_9)_4$	10^4	0.09	[26]
Modified sol-gel with hydrothermal process	$Ca(NO_3)_2 \cdot 4H_2O$, Cu $(NO_3)_2 \cdot 4H_2O$, TiO $(OC_3H_7)_4$	-	-	[30]

synthesis methods are showed as well as their influence on permittivity (ε') and loss tangent (tan δ). From Table 1, microwave synthesis showed the highest value of dielectric constant (ε' = 53,300) but at the same time the highest dielectric loss (tanδ = 0.2), which limit its industrial application. In the next section, the different approaches used for the sintering of CCTO will be reviewed.

3. Sintering and Dielectric Properties

Sintering (Figure 13) is a well-established process used to consolidate powders by heating green bodies at high temperatures below the melting temperature of the powder. It is a thermal treatment for bonding particles into a coherent, predominantly solid structure via mass transport events that often occur on the atomic scale. The bonding leads to improve strength and lower system energy. Most industrial sintering is pressure less and performed without any external applied pressure. Pressure assisted sintering techniques include many processes: hot isotactic pressing, hot pressing, flash sintering and Spark Plasma sintering.

There are challenging demands from all the industries involved in nanotechnology for new and improved sintering process with fine microstructure and enhanced mechanical, electrical, optical and physical properties. The aim of modern ceramic technologies is obtaining dense ceramic with nanostructured grains. That is why there are many factors to be optimized during the sintering process, starting from powders (shape and size of grains), green bodies manufacturing (dimensional changing during compacting which is dependent from the pressure) and sintering type and time.[33] In this review, we will present four main methods of sintering used to obtain dense ceramic of $CaCu_3Ti_4O_{12}$ such as conventional sintering, microwave sintering, spark plasma sintering and thermobaric treatment.

3.1. Conventional Sintering

The conventional sintering process consists of heating a preformed powder (raw or blended materials) at high temperatures, lower than the melting point, during minutes to hours. The driving force for sintering comes from the high surface energy and curved surface inherent to a powder. There are different "stages" for sintering. A "stage" of sintering can be described as an interval of geometric change in which the pore shape change is totally defined or an interval of time during which the pore remains constant in shape while decreasing in size. The sintering process can be divided into three different stages:

- **The initial stage**: Sintering initially causes the particles that are in contact to form grain boundaries at the point of contact through diffusion. The neck and grain boundaries are formed during this stage. Neck formation is driven by the energy gradient resulting from the different curvatures of the particles and the neck. Surface diffusion is usually the

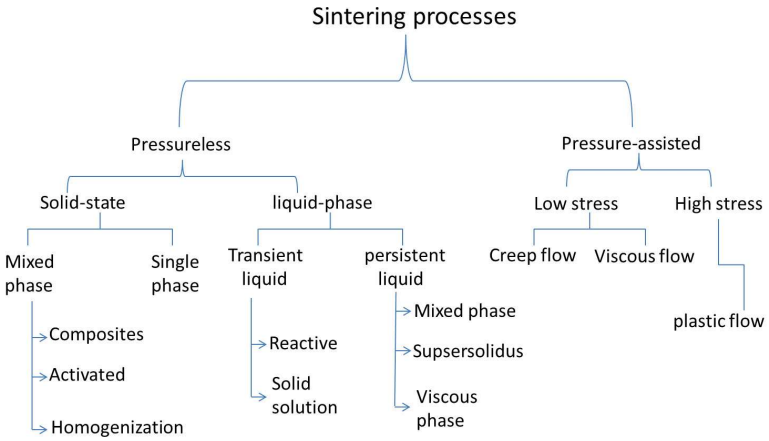

Figure 13. The taxonomy of sintering, showing process differentiation by various branches, starting with the application of pressure-assisted versus pressureless sintering. Adapted from [32]

dominant mass-transport mechanism during the early stages of neck growth, as the compact is heated to the sintering temperature. A smoothing in the surface occurs.

- **The intermediate stage**: During this stage, there is the creation of isolated pore structures. Grain growth and densification occur at this stage too. Densification is assumed to result from pores simply shrinking to reduce their cross section. The intermediate stage normally covers the major part of the sintering process, and it comes to an end when the density of the porous body reaches close to 90% of the fully dense body.
- **The final stage**: Final stage sintering is much slower than the initial and intermediate stages. During this stage, pore shrinkage and closure happen. Pore shrinkage is one of the most important stages in the sintering process. For this shrinkage to occur, solids must be transported into the pores and the gas present inside the pore must escape to the surface. In the final stage, grain growth occurs.

CCTO was widely prepared by conventional sintering and the electrical properties of the obtained ceramics were extensively studied. Different furnaces types were used to a conventional sintering such as refractory type electrical resistance furnace, induction furnace or fossil fuel furnace. High temperature and long sintering duration are maintained during sintering process. During heating, the temperature is distributed between elements by the mechanism of conduction, radiation and convection. First the material surface is heated then heat is transferred into material leading to a temperature differences between the surface and inside the material.[34]

Sinclair *et al.*[7] prepared the CCTO powders via the mixed oxide route using $CaCO_3$, CuO and TiO_2 as starting materials. Pellets were prepared by sintering cold-pressed compacts in air at 1000–1100 °C and were 89 to 90% of the theoretical density. The obtained ceramics showed values for permittivity higher than 10000. The authors explained that the electrical properties of $CaCu_3Ti_4O_{12}$ ceramics depend on many variables, including ceramic microstructure (average grain size and pellet density) and processing conditions (oxygen partial pressure, sintering temperature and cooling rate).

Barbier *et al.*[35] prepared CCTO ceramics by adding an organic binder to the powder and the obtained mixture was pressed into pellets of 6 mm in diameter and 1.5 mm thick, at a pressure of 620 MPa. The obtained pellets were sintered in air at 1100 °C for 24 h. The density of the samples was approximately 4.8 $g\,cm^{-3}$. The pellets exhibited a bimodal grain size distribution (Figure 14).

High values of dielectric permittivity and low losses were observed whatever the electrode ($\varepsilon_r = 1.4\times10^5$ and tg $\delta \sim 0.16$ at 1 kHz). Lukenheimer *et al.*[36] studied the origin of the colossal dielectric constants of CCTO ceramics prepared by conventional sintering. They performed detailed dielectric measurements on various CCTO samples subjected to different surface and heat treatments. The ceramics were sintered at 1000 °C in air for up to 48 h. The authors concluded that there must be two different types of insulating layers in CCTO.

Ferrarelli *et al.*[37] undertook impedance spectroscopy study of CCTO single crystals and CCTO ceramics. The authors

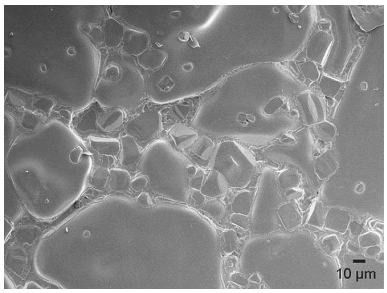

Figure 14. FEG-SEM micrograph of a 6 mm diameter CCTO pellet sintered at 1100 °C for 24 h. Reprinted with permission from (Barbier et al., 2009). Copyright 2009 Elsevier.[35]

mentioned that the impedance spectroscopy is a useful technique to characterize electrically heterogeneous materials and can, in many circumstances, be used to identify and separate intrinsic (e.g. bulk) and extrinsic (e.g. grain boundary, non-ohmic electrode contact) effects. The CCTO ceramics were prepared by uniaxially cold pressing of the CCTO powder into 5 mm compacts under an applied pressure of 50 MPa, followed by pressing at 200 MPa in a Flow Autoclave System model 32330 cold isotactic press. Resulting green body compacts were placed on Pt foil and sintered at 1100 °C for 6 h. Heating and cooling rates of 5 $°C\cdot min^{-1}$ were used for both the powder production and for sintering pellets. CCTO ceramics with a theoretical density of 96% were obtained. The authors observed a predominantly grain boundary effect (IBLC) for ceramics and an extrinsic electrode – sample interface effect for single crystals.

Fiorenza *et al.*[38] used the combination of scanning impedance microscopy and conductive atomic force microscopy on single crystals of the perovskite-type oxide $CaCu_3Ti_4O_{12}$ (CCTO) in order to provide a local dielectric characterization on ingot sections. The authors sintered the single crystals in air for 12 h at 1000 °C. They demonstrated the presence of insulating inclusions in $CaCu_3Ti_4O_{12}$ single crystals, identified to be $CaTiO_3$. The $CaTiO_3$ secondary phase could block/restrict conduction within $CaCu_3Ti_4O_{12}$ crystals and could participate in the macroscopic conduction mechanisms.

Schmidt *et al.*[39] synthesized powders of various compositions within the ternary CaO–CuO–TiO_2 phase diagram from different amounts of dried high purity reagents of $CaCO_3$, CuO and TiO_2. For each composition, pellets were pressed from freshly crushed and ground powders using a uniaxial hydraulic press (1 ton) and all were simultaneously sintered at 1100 °C on Pt foil for 12 h. The authors observed an abnormal increase of the CCTO bulk dielectric permittivity in the absence of CuO secondary phase in the ceramics. Compositions containing CuO phase exhibit increased resistivity.

Turky *et al.*[40] demonstrated that without any dopant, only by controlling the chemistry and engineering, the interfacial regions at the grain boundaries, the dielectric loss can be suppressed remarkably while retaining the giant dielectric constant.

Finally, chung *et al.*[41] prepared pellets sintered in a tube-type furnace at 1100 °C in air for 3 to 20 h and removed immediately to room temperature without any furnace-cooling.

With conventional sintering method, CCTO can be produced in one step of heating, but the use of very high temperature is necessary which is costly in energy domain and non-environmentally.

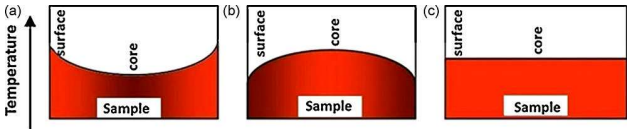

Figure 16. Temperature profile within the sample in: (a) conventional heating, (b) microwave heating and (c) microwave hybrid heating. Reprinted with permission from (Oghbarir et al.,2010). Copyright 2010 Elsevier.[34]

3.2. Microwave Sintering

Microwave sintering is a newly developed technique used for the sintering of materials that has shown many advantages against the conventional sintering process. Microwaves are a form of electromagnetic radiation with wavelengths ranging from about one meter to one millimeter; with frequencies between 300 MHz and 300 GHz. Originally, microwaves were used for communication. Heating of materials with the use of microwave energy got established in 1950. Thus, the microwave heating gained very fast popularity for processing of ceramics, polymers, metallic based materials and advanced materials.

The processing of material using microwaves depends on its dielectric and magnetic properties as the electric field and the magnetic field of the electromagnetic radiation interact with the material during irradiation. The dielectric interaction of materials with microwaves is characterized by two factors: The absorbed power (P) and the depth of microwave penetration (D). The absorbed power in a material is the dissipated power due to the electric and magnetic fields of microwave energy which could be represented as energy converted inside a heated material. Thus, the power absorbed by a material is significantly influenced by the depth up to which the radiations penetrate into it. However, microwaves cannot penetrate inside in the similar fashion in all materials.

Transparent or low dielectric loss materials let the microwaves pass through them without any loss. **Opaque** or conductive materials reflect the microwaves not allowing them to penetrate. Absorbing or high loss materials where microwaves are absorbed depending on the value of the dielectric loss factor (Figure 15).[34,42]

The Basic difference between conventional sintering and the microwave sintering resides in the heating mechanism. (Figure 16) shows the temperature profile for both methods:

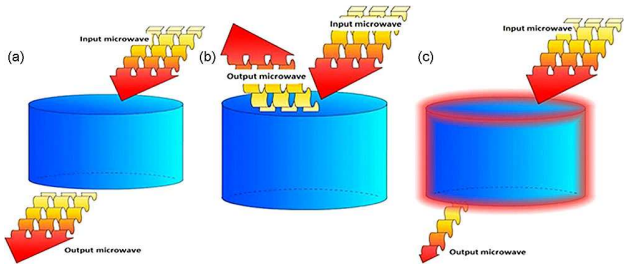

Figure 15. Three kinds of materials according to the interaction with microwaves: (a) transparent, (b) opaque (conductor) and (c) absorber. Reprinted with permission from (Oghbarir et al., 2010). Copyright 2010 Elsevier.[34]

For conventional sintering, heat is generated by heating elements and transferred to samples via radiation, conduction, and convection. In microwave sintering, however, the materials themselves absorb microwave energy, and then transform it into heat within their bodies[34]

The microwave sintering shows many advantages against the conventional sintering process:

- Increased density and more uniform grain sized distribution since it can promote the forward diffusion of ions.
- Lower energy consumption in microwave sintering because the use of microwaves facilitates the transfer of energy directly into the materials, providing volumetric heating.
- Reduced sintering time since microwaves directly interact with the particulates within the green pellets rather than being conducted into the specimen from an external heat source, thereby provide rapid volumetric heating.[34]

Recently many researchers have been using the microwave sintering process to prepare CCTO ceramics.[43,44] In 2016, Kumar *et al.*[43] demonstrated the effect of microwave heating rate on the sintering of CCTO. The higher is the heating rate (50 °C/min) the more uniform and dense is the structure. Conductivity of the obtained ceramics was found to increase with increasing heating rate. They prepared nanocrystalline powders of CCTO by microwave flash combustion technique, the obtained powders were sintered by microwave sintering method. The sintering temperatures were optimized to 1025–1075 °C and the duration to 20 minutes. Figure 17 shows the SEM of the obtained ceramics obtained by microwave sintering.

Thus, the CCTO microstructure has well developed grains and grain boundaries. The grain boundaries are very thin as compared to that of grains. The authors showed that increasing the sintering temperature increases the grain growth in the ceramic as well as the densification (from 94 to 97 %). At room temperature, a giant dielectric constant of 53300 and a small loss tangent of 0.2 at 100 Hz were found in CCTO sample

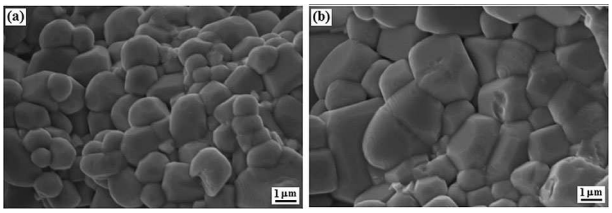

Figure 17. SEM image of CCTO sample sintered by microwave for 20 min at (a) 1025 °C and (b) 1075 °C. Reprinted by permission from (Nature/springer/ Journal of Electroceramics) (Kumar et al.) Copyright (2018).[43]

sintered at 1075 °C for 20 min. It was found that CCTO microstructure was electrically heterogeneous due to grain resistance of 8 Ω and grain boundary resistance of 350000 Ω. This confirms that giant dielectric constant in CCTO is related to inter-barrier layer capacitance.

Ouyang *et al.*[44] used microwave sintering in order to obtain CCTO ceramics. The authors explained that the fundamental difference between conventional sintering and microwave sintering is the difference of the heating mechanisms. The dielectric properties of the ceramics depend on their microstructure. In the microwave sintered samples, an increase in the sintering time decreases the value of the relative permittivity and the electrical loss. While for conventional sintering ceramics, an increase in the time of sintering increase the values of the permittivity and dielectric loss. This difference in behavior between microwave and conventionally sintered ceramics was attributed to the difference in the microstructure.

Raval *et al.*[45] prepared three sets of samples; all of them sintered at 1223 K for 12 h then at 1423 K for 18 h. The first set was slowly cooled, the second one was quenched from the high temperature to liquid nitrogen and the third one was slowly cooled then treated in a domestic microwave (2.45 GHz) for 1 h. They analyzed J-E graphs to investigate the I-V properties of different surfaces resulting from different treatments. They noticed that the maximum current density (J_{max}) decreases from 327 mA/cm^2 for the slowly cooled sample to 254 mA/cm^2 and 234 mA/cm^2 for the quenched and the microwave samples respectively. This behavior was attributed (i) to the relation between surface morphologies (grain size and secondary phases) after quenching and microwave treatment and (ii) to the varistor property.

3.3. Spark Plasma Sintering

Field assisted sintering techniques have become recently very important for the rapid preparation of fully dense ceramic powders. Among them, the novel technique of Spark Plasma Sintering is used for the superfast densification of ceramic nanoparticles within a few minutes. Spark plasma sintering (Figure 18) is a modified hot-pressing process where the ceramic powder compact is placed within a conducting die (mainly graphite), which is in turn heated via high DC or AC electric current density.[46]

The SPS process is performed in partial and low vacuum (* 3 Pa) in order to avoid oxidation of the graphite die at high temperatures. During the process, the sample placed in a conductive matrix and subjected to uniaxial pressure. In this sintering mode, series of DC pulses (pulse duration 3.3 ms, current 0.5 to 8 kA, voltage $\leq$10 volts) are applied during the sintering cycle. By this process it is possible to reach the sintering temperature extremely rapidly with temperature rise rates of up to 600 °C·min^{-1} maximum. As a result, grain growth is strongly inhibited and dense materials of submicron grains can be expected to be obtained at temperatures of about 100 degrees lower than the temperatures required for conventional sintering methods.

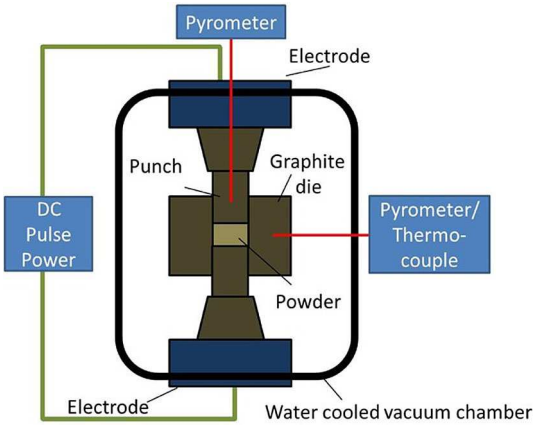

Figure 18. SPS system configuration. Reprinted with permission from (Guillon et al., 2014). Copyright 2014 Creative Commons CC.[46]

Three mechanisms affect the spark plasma sintering, such as enhancement of grain boundaries diffusion process by pulsed current, pressure application and resistance sintering. These three mechanisms have to be optimized in order to obtain a compact structure with grain-to-grain contact.[33]

Kumar *et al.*[47] prepared CCTO ceramics by sintering CCTO powders using the SPS method. The sintering temperature used is 1050 °C and the duration of sintering is 10 min under uniaxial pressure of 50 MPa. The morphology of the particles in the sintered pellet is shown in the Figure 19.

In 2017, Kumar *et al.*[48] obtained spark plasma sintered ceramics using a temperature of sintering of 1050 °C and a duration of 30 minutes. The microstructure of the sintered ceramics (Figure 20a) showed that microstructure has highly compacted grains with grain boundaries. The average grain size is in range of 12–15 μm. The density of sintered sample is measured to 97.5 % of theoretical density.

The frequency dependence of the dielectric constant and loss tangent of SPS sintered ceramics are shown in the following Figure 20b:

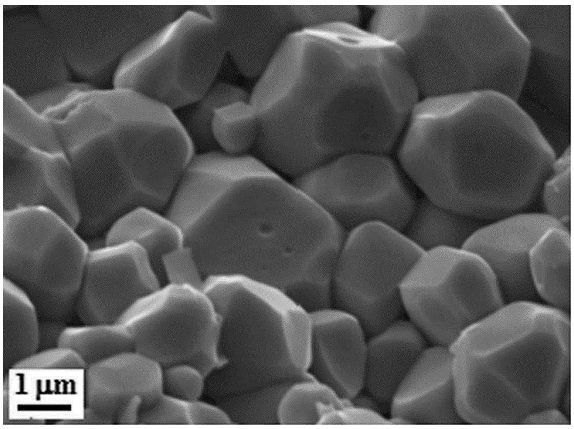

Figure 19. SEM image of CCTO pellets sintered at 1050 °C for 10 min using spark plasma sintering. Reprinted by permission from (Nature/springer/ Journal of Materials science, Materials in Electronics) (Kumar et al.) – *doi.org/10.1007/s10854-015-3275-x* Copyright (2015).[47]

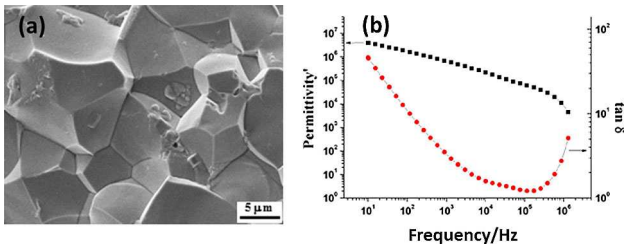

Figure 20. (a) SEM image of fractured CCTO pellet sintered by spark plasma at 1050 °C for 30 min,(b) Frequency dependence of the dielectric constant and tanδ of spark plasma sintered CCTO samples. Reprinted by permission from (Nature/springer/Journal of Materials science, Materials in Electronics) (Kumar et al.) – *doi.org/10.1007/s10854-016-4418-4* Copyright (2016).[48]

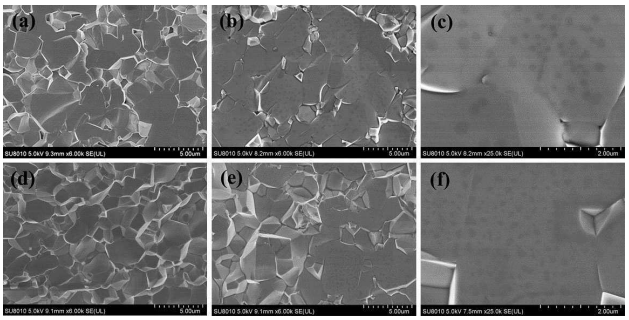

Figure 21. SEM images of fractured cross-sections of CCTO ceramics prepared by SPS method: (a) SPS-900-5, (b) SPS-900-20, (d) SPS-950-5, (e) SPS-950-20 samples; the high magnifications for (c) SPS-900-20 and (f) SPS-950-20 samples with small inclusions. Reprinted with permission from (Lin et al.). Copyright 2018 Elsevier.[50]

Dielectric constant and loss tangent of sintered samples was measured to 1.7×10^6 and 11 at 100 Hz respectively. Using the impedance spectroscopy, the resistance of grain and grain boundary was calculated to be 10 and 190 Ω, respectively. These resistances form the internal resistive barrier that result in a giant dielectric constant in CCTO.

They noticed an increase in grain boundaries resistance. The conductivity shows a nonlinear I-V response that confirmed the non-ohmic electrical grain boundaries properties of CCTO. A polarization is applied between two adjacent CCTO grains (Schottky diode), one of Schottky is forward polarized (semiconductor-insulator) in which the depletion contribution is reduced, and the second one is polarized in reverse (insulator-semiconductor) in which the depletion contribution is enhanced. These two depletions are unequal. By dropping the applied voltage, the reverse side keeps expanding while the forward one is fasten and this behavior results in an increase in width of the depletion region. The decrease of grain boundaries capacitance is induced by the increasing of the width of depletion region and thus non-ohmic electrical grain boundaries properties appears.

Ni *et al.*[49] prepared CCTO spark plasma sintered ceramics and compared them to conventionally sintered CCTO ceramics. In the SPS method, the obtained powders were added in to a graphite die with 12 mm diameter and sintered at temperatures from 750 °C to 950 °C for 5 min under a vacuum of 6 Pa. During the period of heating and soaking, a pressure of 30 MPa was applied to the sample. Then the as-sintered samples by SPS were polished and annealed in air at 800 °C for 2 h to remove the residual carbon on the surface of samples. After annealing, the samples were polished again from both sides to remove the residue from outer layers.

The authors showed that the SPS ceramics showed a higher dielectric constant compared to conventionally sintered ceramics and they attributed this to the higher densification the sintered samples.

Lin *et al.*[50] prepared four different ceramic series that were SPS sintered at 900 °C for 5 min, 900 °C for 20 min, 950 °C for 5 min and 950 °C for 20 min. Figure 21 shows the microstructure of the different ceramics obtained by SPS.

The authors concluded that the ceramics sintered at 900 °C for 5 min have the largest E_b (~9.28 kV/cm) and α (~21.5) value, which can be attributed to the synergistic effects of enhanced barrier height, large activation energy at grain boundaries, and the evolution of microstructure. Spark plasma sintering is an efficient method used to obtain a well and defined structure of CCTO ceramics; however it is a very costly method and not used widely.

3.4. Thermobaric Treatment

High-pressure experimental techniques have been widely used in such fields as mineralogy, petrology, geophysics, and material science. Generally, there are three major high-pressure devices used in high-pressure experimental studies for the Earth and planets, including the piston-cylinder apparatus, the multi-anvil apparatus (MAA), and the diamond-anvil cell (DAC). Each apparatus has its own advantages and unique applications.[51] High pressure and high temperature sintering methods have been recently used to prepare CCTO ceramics.[52,53]

In order to study the properties of the CCTO ceramics prepared by thermobaric treatment, Xu *et al.*[52] prepared quenched CCTO at 1000 °C/10 min after it had been subjected to a high quasihydrostatic pressure of 9 GPa. Such high pressure and high temperature treatment (HPT) result in significant changes of the crystallochemical parameters. The microstructures of the obtained ceramics are shown in Figure 22 (a,b,c,d):

The samples sintered in vacuum show a little larger grain size of ~10 µm than the others, whereas the oxygen sintered samples have more uniform and much finer grain size of about 3–5 µm. Gain boundaries tend to become blurred after thermobaric treatment (TBT).

Figure 22 (e,f,g,h) shows an example of the impedance study done on the ceramics obtained by TBT.

The authors concluded that the grain boundary relaxation is responsible for the abnormal dielectric behaviors of TBT CCTO ceramics. It is affected by the sintering condition and especially TBT processing.

Mao *et al.*[53] prepared the Calcium copper titanium oxide (CCTO) ceramics using the following procedure: Ceramics were quenched in air and liquid nitrogen separately after being

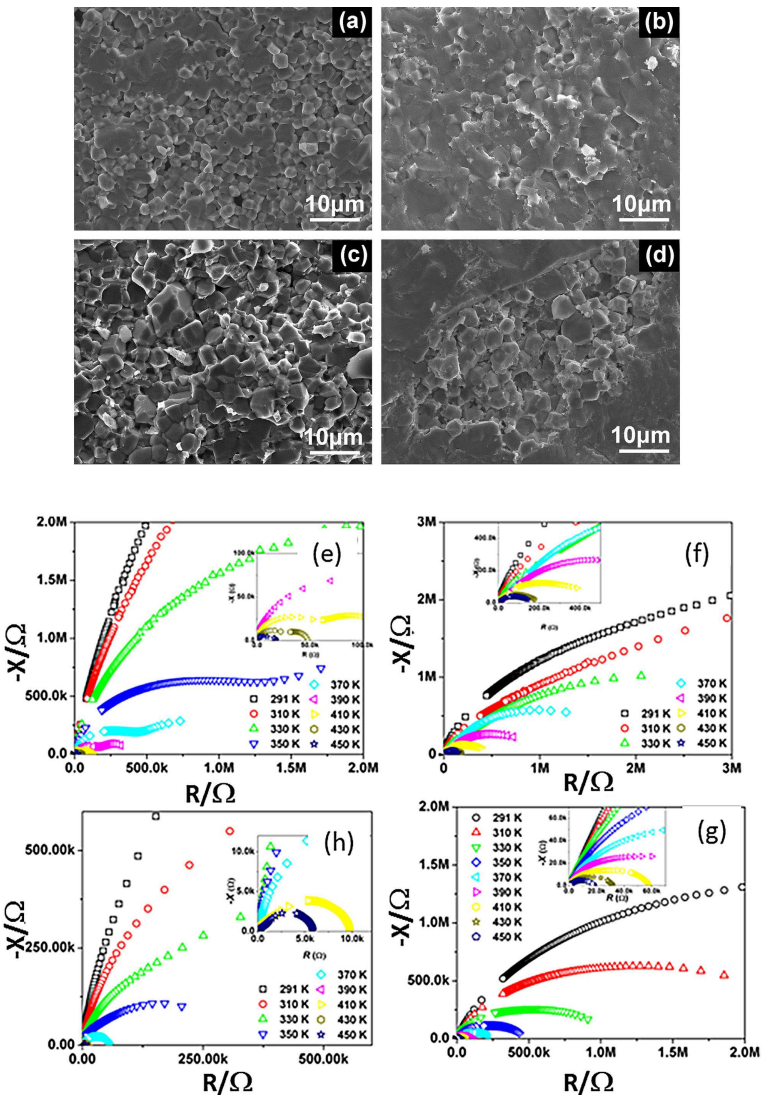

Figure 22. Fracture view field-emission scanning electron microscopy micrographs of (a) O2-CCTO, (b) O2-TBT-LN2, (c) LV-CCTO and (d) LV-TBT-LN2, Complex impedance spectra of CCTO ceramics in the frequency range of 20 Hz–3 MHz at various high temperatures: (e) O2-CCTO, (f) O2-TBT-LN2, (g) LV-CCTO and (h) LV-TBT-LN2. Reprinted with permission from (Xu et al.). Copyright 2018 Elsevier.[52]

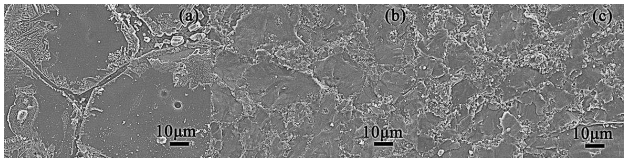

Figure 23. FEG-SEM cross-section images of (a) CCTO, (b) CCTO-TBT-LN2 and (c) CCTO-TBT-Air ceramics. Reprinted with permission from (Mao et al.). Copyright 2018 Elsevier.[53]

subjected to sintering in low vacuum and thermobaric treatment (TBT) at 9 GPa and 1000 °C for 10 min. The microstructures of the obtained ceramics are shown in Figure 23.

The authors observed that after TBT and quenching the grain size decreases tremendously and the grain boundary becomes fuzzy. From impedance study, the authors concluded that the dielectric relaxation of CCTO should be originated with the grain boundary that can be apparently affected by the extreme conditions of TBT and quenching.

It is clear from this section that using different sintering method lead to different microstructures and different dielectric properties as shown in Table 2. Despite the long duration and the high energy used for conventional sintering, this method gives best results of dielectric properties comparing with others, especially for dielectric loss. After reporting the manufacturing methods of CCTO; next section will discuss the insertion of one or two elements into the crystalline lattice in order to investigate their effects on dielectric properties.

4. Doping of CCTO

The first part of this review has shown that copper calcium titanate is a material of choice for the fabrication of ceramic

Table 2. Resuming the sintering method, different temperature and duration used and their influence on permittivity (ε′) and dielectric loss (tanδ).

Sintering method	Precursors	Temperature	ε′	tanδ	References
Conventional Sintering (CS)	$CaCO_3$, TiO_2, CuO	1100 °C/12 h	~10^4	–	[38]
Microwave Sintering	$Ca(NO_3)_2.4H_2O$, $Cu(NO_3)_2.3H_2O$, $C_{16}H_{36}O_4Ti$	950 °C (2.54 GHz,1.25 KW)	3.14×10^3	0.161	[42]
Spark Plasma Sintering	$CaCO_3$, TiO_2, CuO	900 °C/5 min	10^5	–	[46]
Thermobaric Treatment (TBT)	$CaCO_3$, TiO_2, CuO	CS: 1100 °C/24 h TBT:1000 °C/10 min (9 GPa)	10^3	~10	[50]

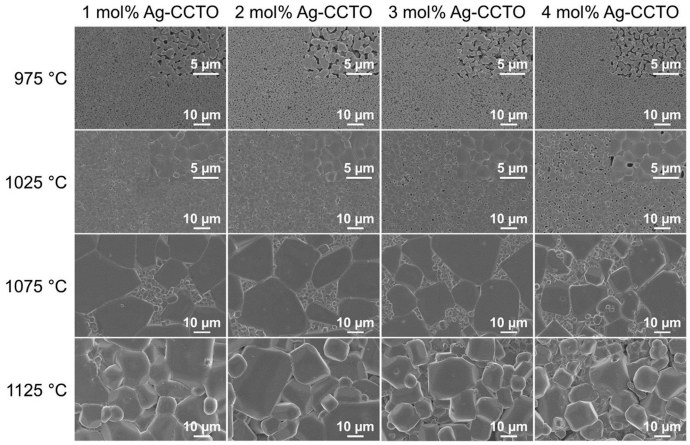

Figure 24. Surface morphologies of 1–4 mol% Ag-doped $CaCu_3Ti_4O_{12}$ ceramics sintered from 975 to 1125 °C for 12 h. Reprinted with permission from (Lee et al.). Copyright 2017 Elsevier.[54]

capacitors because it has an extremely high dielectric constant. The doping of this material by different types of ions can change its electrical properties (relative permittivity, losses, Curie temperature) and lead to other uses. The copper calcium titanate may allow the partial exchange of one, two or three cations by other cations of the same or different valences. It is necessary that the size, charge, and mass of the surrogate ions be compatible with the host site. Doping element or dopant is like an impurity inserted into the element in low concentration to alter some electrical or optical properties, in crystalline materials. These dopants enter into the crystal lattice and take a place of a basic element. Many studies have been performed on the doping of CCTO by different elements and most recently the co-doping of CCTO by two different elements at the same time. This section is divided into two parts, the first one treated the one element doping CCTO and the second part treated the two elements doping.

4.1. Doping of CCTO by One Element

Doping is crucial for determining physical properties and applications for various materials especially semiconductors. Fundamentally, a good dopant should achieve an ideal solubility in its host material and should exhibit a shallow defect level. However, there exist some fundamental doping bottlenecks, which strongly affect the device performance.

In order to enhance dielectric properties, doping CCTO was one of the investigations; it is an insertion of an atom into the structure lattice. Lee *et al.*[54] studied the effect of silver doping on the sintering temperature of CCTO. Ag dopant was added to $CaCu_3Ti_4O_{12}$ powders to reduce the sintering temperature in order to lower the fabrication costs. SEM figures of ceramics obtained from Ag-doped CCTO sintered at different temperatures (Figure 24).

The SEM results indicate that a higher sintering temperature contributes to grain growth and densification, except for the Ag-doped CCTO ceramic specimens sintered at 1125 °C. Ag is believed to behave as a liquid-phase sintering aid. The authors found that the sintering temperature needed for obtaining highly densified ceramics was decreased from 1125 °C to 1075 °C. The relative permittivity of the 2% Ag ceramic increased compared to the undoped CCTO ceramic.

The dependence of current density (J) as the function of the electric field (E) is investigated (Figure 25). They conclude that the leakage of current density increases while doping with Ag atoms (sintered at 1075 °C). At 100 mV, the current density is 1.63 and 0.17 mA/cm^2 for 2% Ag dopant and undoped CCTO respectively.

Xu *et al.*[55] studied the effect of bismuth doping on the electrical properties of CCTO. $Ca_{1-3x/2}Bi_xCu_3Ti_4O_{12}$ (x = 0:0, 0.1, 0.2 and 0.3; BCCTO) ceramics were prepared by traditional solid-state sintering method. They observed a drastic grain size reduction with bismuth doping.

The doping of CCTO by Cobalt was studied by Mu *et al.*,[56] Kafi *et al.*[57] and Wang *et al.*[58]

Mu *et al.*[56] prepared $CaCu_3Ti_{1-x}Co_xO_{12}$ (x = 0, 0.2, 0.4) ceramics by a conventional solid state reaction. Both X-ray diffraction and energy dispersive X-ray spectroscopy confirmed

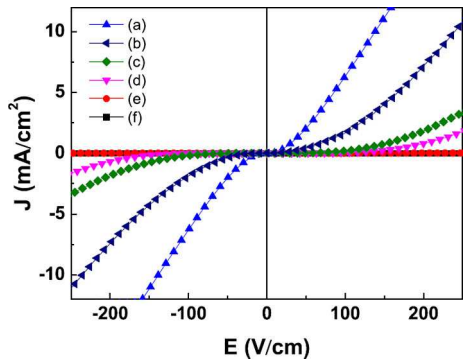

Figure 25. Current density against electric field of (a) 2 mol% Ag-doped $CaCu_3Ti_4O_{12}$ based on nanoparticles sintered at 1075 °C, (b) 2 mol% Ag-doped $CaCu_3Ti_4O_{12}$ sintered at 1075 °C, (c) undoped $CaCu_3Ti_4O_{12}$ sintered at 1125 °C, (d) 2 mol% Ag-doped $CaCu_3Ti_4O_{12}$ sintered at 1125 °C, (e) 2 mol% Ag-doped $CaCu_3Ti_4O_{12}$ sintered at 1025 °C, and (f) 2 mol% Ag-doped $CaCu_3Ti_4O_{12}$ sintered at 975 °C. Reprinted with permission from (Lee et al.). Copyright 2017 Elsevier.[54]

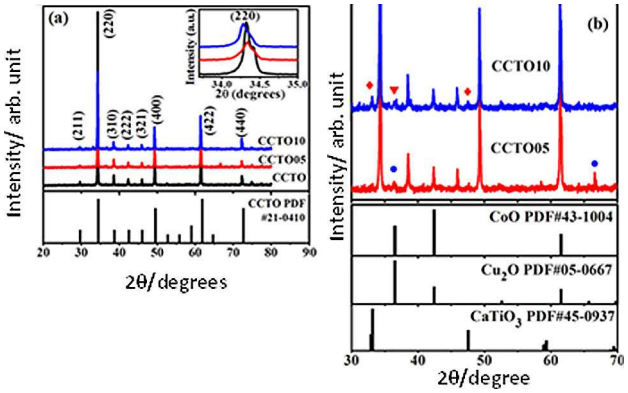

Figure 26. X-ray powder diffraction patterns of (a) CCTO, CCTO05, and CCTO10 ceramics, the top right inset is an expanded view of (220) peaks; (b) expanded XRPD patterns at 2 h$^1/_4$30–70for CCTO05 and CCTO10 ceramics. Reprinted from (Mu et al.) with the permission of AIP publishing.[56]

the presence of Cu and Co rich phase at grain boundaries of *Co*-doped ceramics (Figure 26).

The authors explained that the cobalt can exist in (II) and (III) oxidation states, and can occupy Cu^{2+} and Ti^{4+}, depending on its oxidation state. As compared with Ti^{4+} (r = 0.61 A°), Cu^{2+} (r = 0.57 A°), and Co^{3+} (r = 0.55 A°), Co^{2+} has larger ionic radius (r = 0.75 A° for high spin state). According to the XRD patterns, the authors explained that the Cobalt is replacing the titanium.

Scanning electron microscopy micrographs of Co-doped samples showed a striking change from regular polyhedral particle type in pure $CaCu_3Ti_4O_{12}$ (CCTO) to sheet-like grains with certain growth orientation. The authors showed that the dielectric constant value was slightly changed by 5% and 10% Co doping concentration, whereas the second relaxation process was clearly separated in low frequency region at room temperature. A multi-relaxation mechanism was proposed to be the origin of the colossal dielectric constant.

Kafi *et al.*[57] prepared $CaCu_{3-x}Co_xTi_4O_{12}$ (CCCTO, x = 0, 0.2, 0.4 and 0.6) ceramics using a semi wet method. Their results showed that the dielectric constants of the as-prepared samples in the frequency range of 50 Hz-200 kHz, at room temperature, are reasonably high ($1.7\times10^4 \leq \varepsilon \leq 6\times10^4$). It was also found out that the dielectric loss (tanδ) of the prepared samples decreased by increasing the cobalt concentration at low and middle frequencies.

Wang *et al.*[58] showed that the doping of CCTO by 5% of Co improved the dielectric properties and gave dielectric constant $\varepsilon' \approx 7.4\times10^4$ and dielectric loss $\tan\delta \approx 0.034$ at room temperature and 1 KHz. The authors explained that the Cobalt replaces the Copper ion in the CCTO structure (Figure 27).

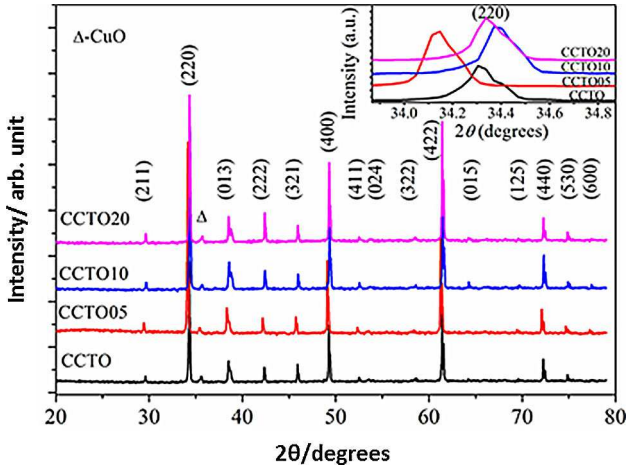

Figure 27. XRD patterns of the pure and various Co-doped CCTO ceramics. Inset shows the enlarged view of the diffraction strongest (220) peak. Reprinted with permission from (Wang et al.) by Oxford University Press and Copyright Clearance Center 2018.[58]

The main XRD peaks correspond to a body-centred cubic CCTO structure with space group Im3 indexed. The secondary-phase peak at ~35.5° ascribed to CuO phase is observed in all tested samples, indicating the precipitation of the liquid CuO-rich phase at GBs. Furthermore, because the absence of CuO phase in CCTO ceramic with 5% Cu deficient is reported elsewhere, the presence of CuO phase in Co-doped CCTO samples preliminarily confirms that the doped Co initially prefers to substitute at the Cu site.

Swatsitang *et al.*[59] prepared $CaCu_{3-x}Cr_xTi_4O_{12}$ (x = 0–0.2) via a polymer pyrolysis route. Best values for the relative permittivity and the loss tangent were obtained for the composition x = 0.08 with a dielectric constant value of 7156 and a low dielectric loss value of 0.092. These values are due to the increase in the grain boundaries resistance caused by the reduction of oxygen vacancies.

The influence of Erbium doping on the electrical behavior of $CaCu_3Ti_4O_{12}$ was studied by Sakthisabarimoorthi *et al.*[60] They prepared pure and Er doped CCTO ceramics by simple sol-gel method. The XRD pattern obtained confirmed that the addition of Er did not affect the crystallinity of CCTO. High dielectric constant ($\varepsilon_r = 26.749$) was found for Er doped $CaCu_3Ti_4O_{12}$ ceramics.

Li *et al.*[61] reported the effect of Europium (Eu) on the dielectric properties of $CaCu_3Ti_4O_{12}$. The experimental results

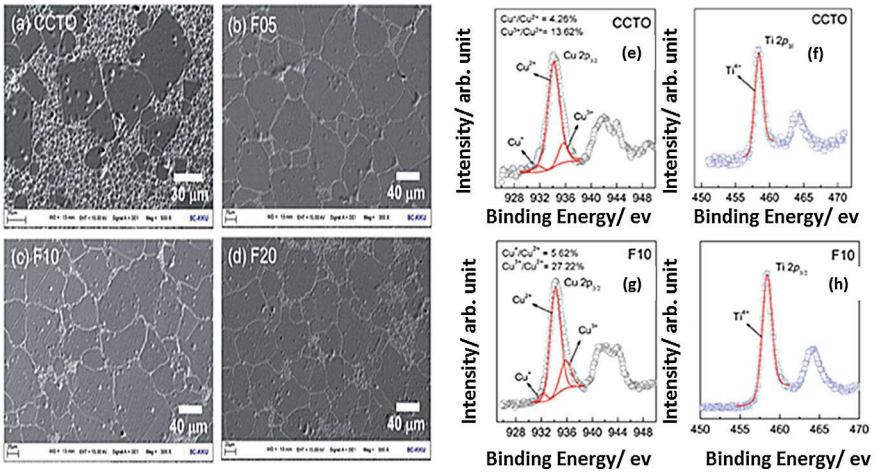

Figure 28. SEM images of polished surfaces of (a) CCTO, (b) F05, (c) F10 and (d) F20 samples, XPS spectra of CCTO and F10 samples: (e, f) Ti 2p regions and (g, h) Cu 2p regions. Reprinted from ref [62] Copyright © 2017 Royal Society of chemistry.

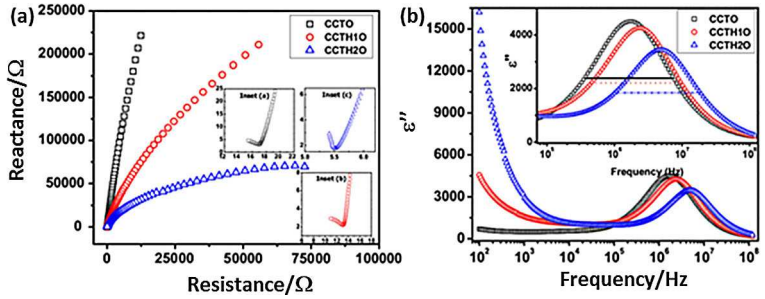

Figure 29. a) Complex impedance plot for all samples. Inset a is showing magnified view of semicircular arcs corresponding to grain contributions (i.e. corresponding to highest probing frequencies) for CCTO, Inset b for CCTH1O and Inset c for CCTH2O. b) Variation of imaginary part of dielectric constant (ε'') as a function of frequency for all samples. Reprinted by permission from (Nature/springer/Journal of Materials science, Materials in Electronics) (Late et al.) – *doi.org/10.1007/s10854-016-4505-6* Copyright (2016).[63]

show that the doping of Eu on a calcium (Ca) site improves the dielectric loss and decreases the dielectric constant of CCTO.The authors explained this result because of the lack of the oxygen vacancies in the samples.

An enhancement of grain growth is produced with F^- doping CCTO studied by Jumpatam *et al.*[62] as shown in Figure 28.

The increase in the dielectric permittivity (98396 for F20) and the decrease of dielectric loss for a factor of 5 ($\tan = 0.1$) is attributed to the effect of F^- that enhances the Schottky barrier height at grain boundaries, in addition to the increase in Ti^{3+} and Cu^+ concentrations (Figure 28e,f,g,h) as a result of charge compensation leading to a large charge polarization space at grain boundaries.

Late *et al.*[63] have investigated the effect of Hf doping on the structural, dielectric and optical properties of CCTO. The authors considered that Hf substitute to Ti sites. From the XRD patterns, they deduced that when the Hf doping exceeds 2% some amount of HfO_2 remains un-reacted in the sample. Furthermore, with in Hf doping both lattice parameters and structural coherency of CCTHO samples increases due to the higher ionic radius of Hf^{4+} compared to the ionic radius of Ti^{4+}. The authors studied the electrical properties using impedance spectroscopy (Figure 29).

They observed that with Hf doping overall grain boundary resistance decreases compared to that of pure CCTO compound. Further, Hf substitution increases dispersion of resistances between grain and the grain boundary. The authors concluded that the shift of relaxation frequency to higher values may be recognized to the decrease in the grain, grain boundary resistance and mean relaxation time. The improved dielectric properties with Hf doping may be credited to the improved structural coherency, increased grain size and optical band gap of these samples. The results agree well with the IBLC model.

The influences of K^+ doping and sintering conditions on the microstructures and dielectric properties were analyzed and discussed by Wang *et al.*[64]The authors observed that the grain size increases with the increasing sintering temperature and K^+ doping concentration.

The authors obtained giant ε′ of $\sim 2.3 \times 10^4$ as well as relatively low tanδ of ~0.039 that can be observed in $Ca_{0.99}K_{0.02}Cu_3Ti_4O_{12}$ ceramics sintered at 1060 °C for 8 h measured at RT and 1 kHz.

Chen *et al.*,[65] Srivastava *et al.*[66] and Huang *et al.*[67] studied the effect of Lanthanum doping on CCTO. Chen *et al.*[65] employed the rare earth element La to replace Ca site and studied the La doping effects on the microstructure and the non-Ohmic properties of La-doped CCTO. From microscopic observations, the authors deduced that the low content of La ions ($x \leq 0.015$) doping hardly affects the crystal structure and the grain size. However, the significant change in microstructure is clearly revealed as $x \geq 0.02$. With the increase of La content, the grain size is remarkably reduced to about 5 μm and the grain boundaries are blurred to obscurity.

The authors also concluded that the nonlinear behavior of CCTO system is not only influenced by the grain size, but also controlled by the local electron density which would affect the chemical environment of defects.

Srivastava *et al.*[66] prepared a 1% La doped CCTO via semi wet route. La doped CCTO showed a slight increase in the value of the dielectric constant compared to undoped CCTO (5000 for undoped CCTO and 7000 for La doped CCTO) at room temperature. Permittivity and dielectric loss increase with increasing temperature for both undoped and doped CCTO. The effects of La^{3+} doped in calcium copper titanate (CCTO) at Ca^{2+} site and Cu^{2+} site were examined by Huang *et al.*[67] The doped compositions, $La_{0.1}Ca_{0.85}Cu_3Ti_4O_{12}$ (LCCTO) ceramics and $CaLa_{0.1}Cu_{2.85}Ti_4O_{12}$ (CLCTO) ceramics were prepared by the solid-state method. Ceramics were prepared under sintering temperatures ranging from 1040 to 1100 °C. The microstructure of LCCTO ceramics presented a bimodal grain growth model (Figure 30).

It was found that La^{3+} doped at Ca^{2+} site achieved lower sintering temperatures than that doped at Cu^{2+} site in CCTO ceramics. The dielectric loss (tan δ) of LCCTO ceramics was about 0.05 at 40 kHz when the sample was sintered at 1080 °C. Dielectric constant (ε′) of LCCTO ceramics was about 3.2×10^4 when the sample was sintered at 1100 °C, which was larger than CLCTO ceramics examined under the same process condition with different sintering temperature.

Mg doped CCTO was studied by Sun *et al.*[68] and Swatsitang *et al.*[69] Sun *et al.*[68] prepared $CaCu_{3-x}Mg_xTi_4O_{12}$ ceramics with high ε′ and very low tanδ by the sol–gel method. Very high values of relative permittivity and low values for dielectric loss were obtained for Mg doped CCTO ceramics : ε′ of 2.52×10^4 and tanδ of ~0.017 at 1 kHz and RT have been achieved for ceramics sintered at 1080 °C for 8 h in the air atmosphere.

Swatsitang *et al.*[69] prepared the nominal $CaCu_{3-x}Mg_xTi_{4.2}O_{12}$ (0.00, 0.05 and 0.10) ceramics by sintering pellets of their precursor powders obtained by a polymer pyrolysis solution method at 1100 °C for different sintering times of 8 and 12 h. Very low loss tangent (tanδ) < 0.009–0.014 and giant dielectric constant (ε′) ~1.1×10^4–1.8×10^4 with excellent temperature coefficient (Δε′) less than ±15% in a temperature range of −60 to 210 °C were achieved. It was found that tanδ values decreased with increasing Mg^{2+} dopants due to the increase of grain boundary resistance (R_{gb}) caused by the very high density of grain, resulting from the substitution of small ionic radius Mg^{2+} dopants in the structure.

Wang *et al.*[70] accomplished a comparative study on the colossal dielectric constant behavior of the pure and Mn-doped $CaCu_3Ti_4O_{12}$ ceramics over a wide range temperature aiming at deeply understanding the role of the Mn doping effects on the physical origin of the colossal dielectric constant behavior. The nominally pure and doped CCTO ceramics by substituting 2% and 4% Mn at Ti sites (abbreviated as CCTO, CCTMO-2, and CCTMO-4, respectively) were prepared using the conventional solid-state reaction method. The resultant materials were sintered at 1100 °C for 10 h. XRD patterns showed a decrease in the lattice parameters and SEM micrographs showed that Mn doping is beneficial for grain growth (Figure 31).

Concerning the dielectric studies, the authors concluded that Mn doping is harmful for the CDC behavior and they attributed this to the decrease in the ratios of Ti^{3+}/Ti^{4+} and Cu^{3+}/Cu^{2+} and the concentration of oxygen vacancies. Their

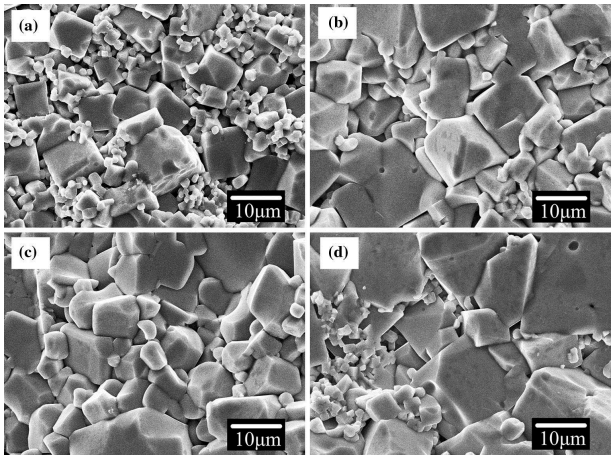

Figure 30. SEM images of the surface morphologies of LCCTO sintered at a 1040 °C, b 1060 °C, c 1080 °C, d 1100 °C for 10 h. Reprinted by permission from (Nature/springer/Journal of Materials science, Materials in Electronics) (Huang et al.) – *doi.org/10.1007/s10854-016-5244-4* Copyright (2016).[67]

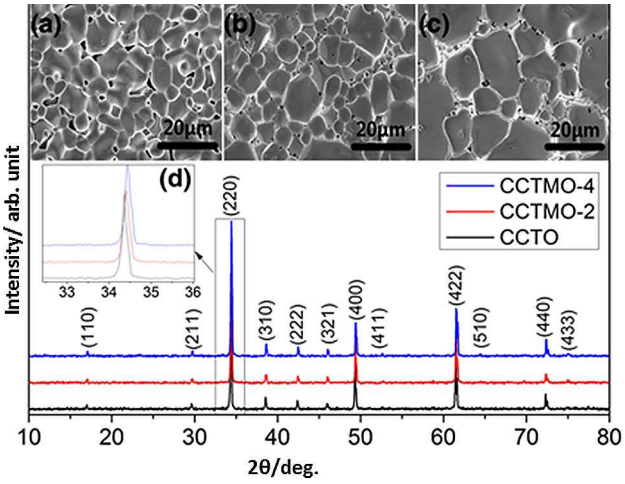

Figure 31. XRD patens of CCTO, CCTMO-2, and CCTMO-4 ceramics. Inset shows the SEM micrographs of (a) CCTO, (b) CCTMO-2, (c) CCTMO-4, and (d) the enlarged view of the (220) reflection peaks. Reprinted by permission from (Nature/springer/Journal of Electroceramics) (Wang et al.) – *doi.org/10.1007/s10832-016-0024-3* Copyright (2016).[70]

results confirm the multi-relaxation mechanism for the CDC behavior in CCTO and the CDC behavior is mainly dominated by Maxwell-Wagner contribution.

The perovskite-type $CaCu_3Ti_4O_{12}$ (CCTO) doped by molybdenum (Mo) and its dielectric properties and the temperature dependence of Electron Spin Resonance (ESR) has been investigated by Kouassi *et al.*[71] Substitution on Ti-site by Mo helps to increase the grain size of samples and therefore increase the dielectric constant according to the IBLC theory. There is no great difference between the ESR spectra of pure CCTO and CCTO doped by Molybdenum as a function of temperature (Figure 32).

Nickel doped CCTO were prepared and studied by Senda *et al.*,[72] Wang *et al.*,[73] Boonlakhorn *et al.*[74] and Sun *et al.*[9]

In the aim of increasing the relative permittivity and decreasing the dielectric loss of CCTO, Sun *et al.*[9] prepared $CaCu_{3-x}Ni_xTi_4O_{12}$ (x = 0, 0.05, 0.1, 0.2) powders by the sol-gel method. The pellets were sintered at 1000–1060 °C for 8 h. A very low tanδ value ~0.025 was found at the $CaCu_{2.95}Ni_{0.05}Ti_4O_{12}$ ceramic sintered at 1060 °C for 8 h with $\varepsilon' \sim 4.2 \times 104$ at about 1 kHz. Senda *et al.*[72] studied the influence of Ni doping on $CaCu_{3-x}Ni_xTi_4O_{12}$ (x = 0,0.05,0.075,0.1,0.2,0.3) ceramics sintered at 1100 °C for 6, 12 and 24 h in air. After sintering for 12 h, they obtained for $x \leq 0.2$ the pure phase and for $x > 0.2$ $CaTiO_3$, TiO_2 and CuO as a secondary phase. The highest dielectric permittivity was recorded to the composition x = 0.2 (10^5) with a slight decrease in loss tangent. Doping element enhance the cubic grain growth as shown in (Figure 33). Dielectric properties of all composition showed a dependence of frequency range. At high frequency (1 kHz) the permittivity and loss tangent decrease.

Wang *et al.*[73] reported good dielectric properties, a dielectric permittivity of $\sim 1.5 \times 10^5$ and a low loss tangent of ~0.051, were obtained by optimization of dopant levels ($CaCu_{2.80}Ni_{0.20}Ti_4O_{12}$) and sintering conditions (1100 °C for 3 h).

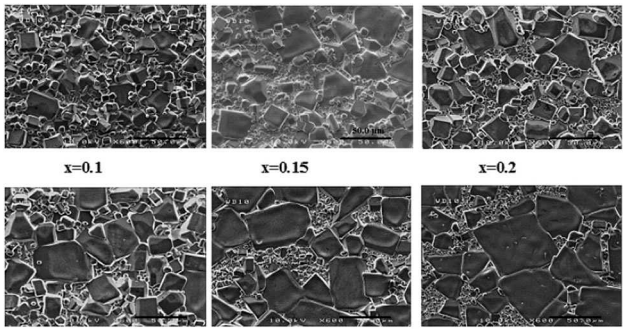

Figure 33. SEM images of surface morphologies of pure and Ni doped samples sintered at 1100 °C for 12 h. Reprinted from (Senda et al.). Copyright 2017 Elsevier.[72]

Boonlakhorn *et al.*[74] found that doping CCTO with Ni^{2+} caused a great increase in its dielectric permittivity, by a factor of ~3.

Li *et al.*[75] fabricated $CaCu_{3-x}Ru_xTi_4O_{12}$ (x = 0, 0.03, 0.05 and 0.07) electronic ceramics. They noticed an inhibition of grain growth after doping with Ru. In general, during the sintering treatment, a liquid phase of Cu is formed at grain boundaries and ions diffuse through it to form a large grain. The authors performed EDX analysis on the grain boundaries, and they found that for pure CCTO, Ti, Ca, O and Cu ions are present in excess in the grain boundary region, while for Ru-doped CCTO, Ti and Ca atoms were the ones present in excess. It is well known that TiO_2 and CaO have high melting point and inhibit the formation of a liquid phase during the sintering process.

When doped with proper amount of Ru (x = 0.05), CCTO displays low dielectric loss (tan $\delta < 0.05$), while simultaneously maintains a decent dielectric constant ($\varepsilon > 80$).

Cortes *et al.*[76] focused on CCTO doped with Sn^{4+}, $Ca_2Cu_2Ti_{4-x}Sn_xO_{12}$ ($0.0 < x < 4.0$). They reported that the materials with low Sn^{4+} contents (x = 0.1 and 0.2) presented giant dielectric permittivity values, 166381 and 140845 respectively.

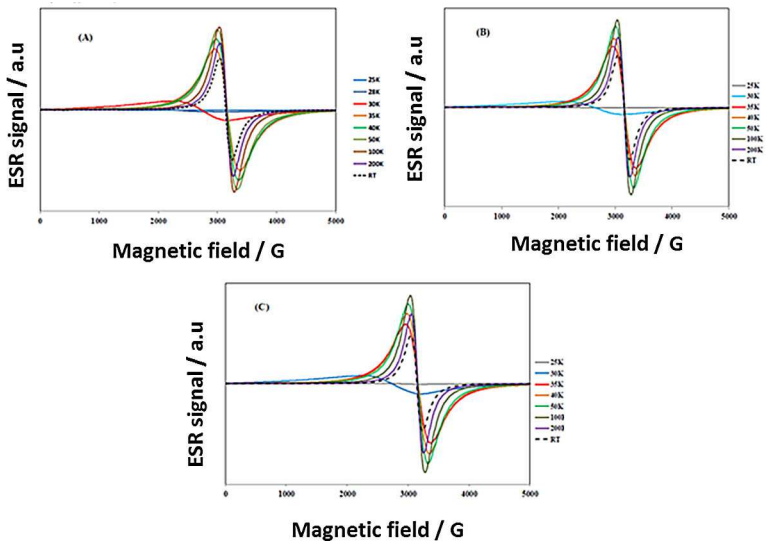

Figure 32. Temperature dependence of ESR for pellets sintered at 1050 °C of M0 (a), M0.05 (b) and M0.1 (c). Reprinted from (Kouassi et al.). Copyright © 2017Creative commons.[71]

They associated this to insulating grain boundaries with activation energies of 0.58 eV and 0.30 eV respectively, as well as conductive grains with activation energies of 0.04 eV and 0.08 eV.

Sahu *et al.*[77] investigated the effect of doping type on conduction and dielectric phenomena in 15% Sr doped CCTO. The Maxwell–Wagner model and interfacial polarization explains the higher dielectric constant of the material at higher temperatures.

Amhil *et al.*[78] recently prepared 0.05 Sr doped CCTO via a semi wet chemical route. Microstructural study showed that Sr concentration promotes grain growth in CSCTO ceramics. The dielectric properties were enhanced by the doping.

Tungsten doped CCTO was investigated by Singh *et al.*[79] $CaCu_3Ti_{4-x}W_xO_{12}$ (x = 0.01, 0.03, and 0.05) ceramics were prepared by flame synthesis method. The dielectric property measurement shows that the relative permittivity (ε_r)and dielectric loss (tanδ) values in the measured frequency range at 328 K for W-doped ceramics were increased with increasing W content.

Kouassi *et al.*[80] again studied the effect of vanadium doping on the microstructure and dielectric properties of CCTO. They reported that the vanadium doping of CCTO system results in an increase of grain size, the grains being surrounded by melted-like grain boundaries. They added that in doped samples, above 1 kHz, a relaxation appears which is evidenced by a drop of real part of permittivity and a peak of its imaginary part. This relaxation phenomenon is very significant at relatively low doping rates and then decreases again as vanadium content increases.

Tang *et al.*[81] focused on the enhancement of dielectric properties of Y^{3+} donor doped CCTO. Grain growth in $Ca_{1-x}Y_xCu_3Ti_4O_{12}$ was suppressed with increasing the concentration of dopant element.

The permittivity increases (8.03×10^4) for x = 0.05 at 1 kHz and loss tangent decrease to 0.05 for x = 0.03 in a frequency range between 1.5 kHz and 60 kHz. Figure 34 presents the relationship between dielectric constant and grain resistance in CYCTO ceramics in order to explain the dependence of increasing the dielectric constant and the grain growth.

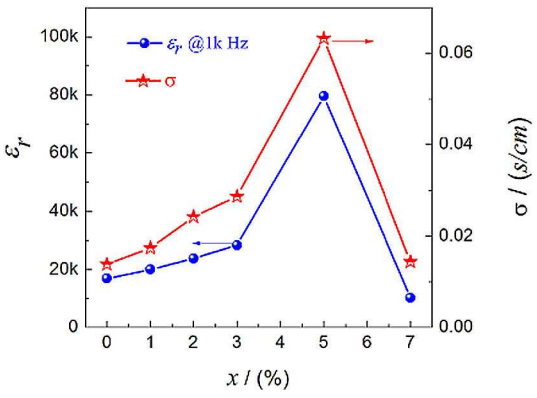

Figure 34. Relationship of dielectric constant (1 kHz) and Grain resistance in $Ca_{1-x}Y_xCu_3Ti_4O_{12}$ ceramics. Reprinted from (Tang et al.). Copyright 2018 Elsevier.[81]

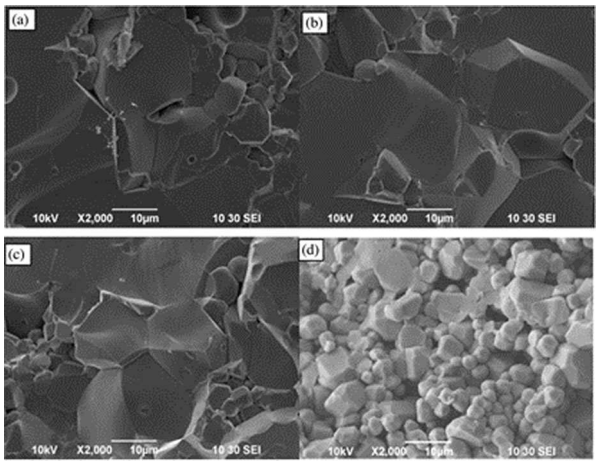

Figure 35. SEM images of fracture morphologies for (a) pure CCTO, (b) Y-doped CCTO, (c) Zr-doped CCTO, (d) Ta-doped CCTO. Reprinted from (Xue et al.). Copyright 2016 Elsevier.[82]

Xue *et al.*[82] studied the doping of CCTO by different elements such as Y, Ta and Zr. They found that the grain growth changed with different doping element (Figure 35) even the dielectric properties are different. For Y^{3+} doped CCTO, the dielectric constant increases and nonlinear property decreases while doping with La^+ leads to inverse results. Doping by Zr^{2+} leads to the same results given for pure CCTO.

Gonzales *et al.*[83] presented the results of Zr oxide doping of a $CaCu_3Ti_4O_{12}$ (CCTO) ceramic prepared by a solid-state reaction. Zr-doping controls the grain size growth, leading to a reduction of the grain size. For both dopant concentrations of 0.5 and 1 wt.%, all of the samples exhibited lower dielectric loss and a smaller dielectric constant than those of undoped CCTO. The sample doped with 0.5% of the non-stoichiometric ZrO exhibits a dielectric constant over 3200 and a dissipation factor of 0.02 at 1 kHz.

Xu *et al.*[84] reported a very high dielectric permittivity value of 7591 and a very low tanδ value of 0.023 at 1 kHz for $CaCu_3Ti_{3.8}Zr_{0.2}O_{12}$.

All obtained results are resumed in Table 3. Based on these results, F^- dopant element exhibits the highest dielectric properties where ε = 81,306 and tanδ = 0.07. These can be caused due to the increase of grain boundaries resistivity and decrease of grains resistivity. Improvement of dielectric properties can be explained by the presence of free charge carrier concentration inside the semiconducting grains and Schottky barrier height at the grain boundaries respectively. A stronger intensity of interfacial polarization (Maxwell-Wagner polarization) is due to high charges concentration accumulated at the interface between grains and grain boundaries under an applied electric field.[62]

4.2. Co-Doping of CCTO by Two Elements

In general, co-doping can be efficient for increasing the dopant solubility, increasing the activation rate by lowering the

Table 3. dopant element, concentration, permittivity, loss tangent (tanδ) and grain size of doped CCTO ceramic.

Dopant	Concentration	ε_r (10^3 Hz)	tanδ (10^3-10^6)	Grain size	References
Ni	x = 0.2	$>10^5$	10^{-1}	50 μm	[85]
Cr	x = 0.08	7,156	0.092	60.3 μm	[59]
Y	x = 0.5	$8.03*10^4$	~0.01	2-4 μm	[81]
Co	5%	$7.4*10^4$	0.034	48.5 μm	[58]
Er	x = 0.1	26,749	–	200 nm	[60]
Sr	x = 0.2	$>10^4$	~0.3	~20 μm	[86]
Co	x = 0.6	6×10^4	0.15	75 μm	[57]
SnO_2	2 mol%	~21,250	0.04	3–5 μm	[87]
Mg	x = 0.1	$\sim2.52\times10^4$	0.017	~2-20 μm	[68]
Y	x = 0.05	~31,125	~0.14	~55 μm	[82]
Zr	x = 0.05	~22,260	~0.02	~32 μm	[82]
Ta	x = 0.05	~17,500	~0.01	~4 μm	[82]
Mg	x = 0.05	$\sim3\times10^4$	~0.013	~45.65 μm	[88]
Y	x = 0.05	$\sim8\times10^3$	~0.013	~2.52 μm	[88]
Sn	x = 0.2	140,845	0.71	4.17 μm	[76]
Nb	x = 0.025	4.8×10^5	0.566	~20.2 μm	[89]
Al	x = 0.025	2.1×10^5	0.129	~129.6 μm	[89]
Y	x = 0.02	32,000	0.05	1–2 μm	[90]
Sr	x = 0.4	$\sim2\times10^4$	~1.0	2.7 μm	[91]
La	x = 0.15	$\sim5\times10^3$	~0.1	3.9 μm	[91]
Zr	x = 0.5	3,200	0.02	3.6 μm	[83]
F^-	x = 0.1	81,306	0.077	~40–100 μm	[62]
Ru	x = 0.7	$\sim6.0\times10^3$	~0.4	2–4 μm	[75]
LiF	0.5%	34,994	0.68	2.1 μm	[92]
Mn	2%	3.0×10^3	–	7–9 μm	[70]
K	x = 0.01	2.3×10^4	0.039	4.28 μm	[64]
Yb-6 h	x = 0.05	9,832	0.014	~2–6 μm	[93]
Yb-12 h	x = 0.05	16,033	0.015	20–50 μm	[93]

ionization energy of acceptors and donors, and increasing the carrier mobility.[94] CCTO was largely doped with single elements but most of the heteroatomic substitutions that are employed to improve a dielectric property of the CCTO always worsen simultaneously another dielectric performance. This is the reason why many researchers are trying to perform co-doping on CCTO.

Boonlakhorn *et al.*[88] improved the dielectric properties of $CaCu_3Ti_4O_{12}$ by co-doping with Y^{3+} and Mg^{2+} to simultaneously control the geometric and intrinsic properties of grain boundaries (GB), respectively. The authors found that the substitution of these dopants strongly suppressed the grain growth while enhancing the resistivity of an individual GB, respectively. This led to a great decrease in the loss tangent (tanδ ~ 0.013).

The authors prepared $Ca_{0.925}Y_{0.05}Cu_{2.95}Mg_{0.05}Ti_4O_{12}$ (Y–Mg05) using a modified sol-gel method. The obtained compacted powders were sintered in air at 1070 °C for 6 h using heating and cooling rates of 5 °C/min.The authors deduced that the resistance of the grain boundaries is increased by the addition of dopants.

The same authors doped CCTO by both Al^{3+} and Nb^{5+}.[89] They found that the substitution of (Al^{3+}, Nb^{5+}) co-dopants into TiO_6 octahedral sites of $CaCu_3Ti_4O_{12}$ ceramics, which were prepared by a solid state reaction method and sintered at 1090 °C for 18 h, can cause a great reduction in a low-frequency loss tangent (tanδ ≈ 0.045–0.058) compared to those of Al^{3+} or Nb^{5+} single-doped $CaCu_3Ti_4O_{12}$.

The authors deduced that the doping with Nb^{5+} reduces the grain size while doping with Al^{3+} results in a large increase in the mean grain size. Alternatively, the mean grain sizes of the co-doped NA025 and NA05 ceramics were between the mean grain sizes of the single-doped Al025 and Nb025 ceramics and not much different that of the un-doped CCTO ceramic. They concluded that the simultaneous substitution of both Al^{3+} and Nb^{5+} ions can balance the driving and restorative forces for grain boundary (GB) migration.

The ε′ values of the single-doped Al025 and Nb025 ceramics are larger than those of the co-doped NA025 and NA05 ceramics. Nevertheless, ε′ values of both co-doped ceramics are still too large ($>10^4$). Interestingly, over the measured frequency range, the tanδ values of both co-doped ceramics are much lower than those of the single-doped ceramics as well as the un-doped CCTO ceramic.

The co-doping of CCTO by Al^{3+} and Nb^{5+} was also studied by Wen *et al.*[95] The authors concluded again a decrease in the dielectric loss of ceramics after codoping.

Boonlakhorn *et al.*[96] studied the dielectric properties of Sm and Zn codoped $CaCu_3Ti_4O_{12}$ ceramics. The values of the electrical permittivity and the loss tangent obtained for the different ceramics are shown in Table 4.

The authors observed that the ε′ and tan δ values of the Sm05, SmZn05 and SmZn10 ceramics were lower than that of the CCTO ceramic over the measured frequency range. It should be noted that the low-frequency tanδ value of the single-doped Sm05 ceramic was much higher than that of the un-doped CCTO ceramic, while simultaneous substitution of Sm and Zn dopants into CCTO ceramics caused a great decrease in tanδ over the measured frequency range.

Ren *et al.*[97] co-doped $CaCu_3Ti_4O_{12}$ by Al^{3+} and Bi^{3+} elements to improve the electrical properties and enhance the varistor

Table 4. dopant element, concentration, permittivity, loss tangent (tanδ) and grain size of doped CCTO ceramic.

Material	Concentration	εr (10^3 Hz)	tanδ(10^3–10^6)	Grain size (μm)	References
Y^{3+}/Al^{3+}	0.05	20×10^4	0.048	2–5	[105]
Bi/Al	1% mol	4,020	10^{-1}	2.29–3.24	[97]
Sr/Ni	X = 0.1/0.1	44,410	0.07	35.50	[108]
Sr/Zn	x = 0.05/0.1	29,664	0.049	0.74	[103]
La/Zn	Zn (5–10%)	8,102	0.1	3–4	[99]
Y^{3+}/Zn^{4+}	3 mol%/5 mol %	10,196	~0.039	1.3–3.5	[106]
Sm/Zn	x = 0.05/0.1	5,313	0.041	~2	[96]
Mg/Y	x = 0.05/0.05	$\sim10^4$	~0.013	~3.73	[88]
Nb^{5+}/Al^{3+}	x = 0.025	4.1×10^4	0.058	~35.1	[89]
Nb^{5+}/Al^{3+}	x = 0.05	2.9×10^4	0.045	~34.6	[89]
Mg/Y	x = 0.05/0.05	$\sim10^4$	~0.013	~3.73	[88]
Nb^{5+}/Al^{3+}	x = 0.025	4.1×10^4	0.058	~35.1	[89]
Nb^{5+}/Al^{3+}	x = 0.05	2.9×10^4	0.045	~34.6	[89]
Sr/La	x = 0.4/0.15	$\sim4\times10^4$	~0.05	0.6	[91]
Ni^{2+}/Zr^{4+}	x = 0.05/0.1	$\sim2\times10^4$	0.026	4.75	[104]
LiF	0.5%	34,994	0.68	2.1	[92]
Yb/Mg	x = 0.05/0.3	$\sim10^4$	0.018	2.32	[107]
FeNb	x = 0.5	8.0×10^4	~0.8	1.9	[98]

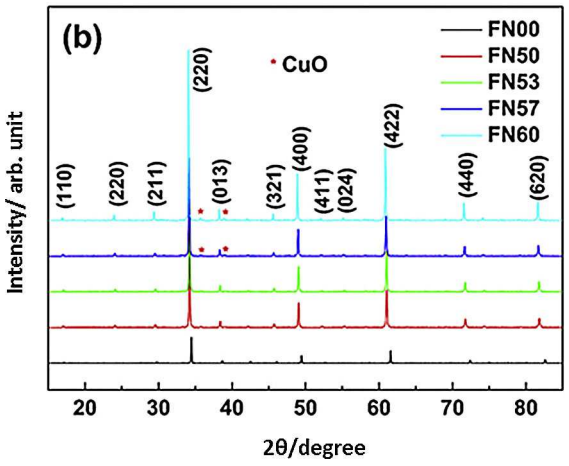

Figure 36. XRD patterns of $CaCu_3$ $(Ti_{1-x}Fe_{x/2}Nb_{x/2})_4O_{12}$ powders with different percentage of codoping. Reprinted from (Bai et al.). Copyright 2016 Elsevier.[98]

property of CCTO. The authors observed that the grain size homogenization was enhanced with co-doping. Although the average grain size shows not much difference, the grain size distribution of co-doped sample is much more uniform with smaller variance. The authors reported an enhancement of dielectric properties and varistor properties for 1 mol% doping concentration. An increase of dielectric permittivity and decrease of dielectric loss to 0.04 at low and medium frequencies could be attributed to an increase of activation energy of dc conductance at grains boundaries as well as improvement in grains boundaries resistivity.

Bai *et al.*[98] prepared the $CaCu_3$ $(Ti_{1-x}Fe_{x/2}Nb_{x/2})_4O_{12}$ (x = 0.00, 0.50, 0.53, 0.57, 0.60) ceramics through the solid state reaction method with the pre-synthesis of the monoclinic precursor $FeNbO_4$.

From Figure 36, it has been noticed that the $CaCu_3$ $(Ti_{1-x}Fe_{x/2}Nb_{x/2})_4O_{12}$ powders kept single phase up to a codoping concentration of $(Fe_{1/2}Nb_{1/2})^{4+}$ complex ions as high as 60%. The dielectric frequency spectra of $CaCu_3$ $(Ti_{1-x}Fe_{x/2}Nb_{x/2})_4O_{12}$ ceramics reveals the existence of Debye-type relaxations in measurement frequency range.

The effect of the addition of La and Zn on the dielectric properties of CCTO was studied by Rani *et al.*[99] They prepared $Ca0_{.95}La_{0.05}Cu_{3-x}Zn_xTi_4O_{12}$ (x = 0.01, 0.025, 0.05 & 0.10) by conventional solid state technique. The ceramics were sintered at 1080 °C for 6 hours with 5 °C/min rate of heating and cooling. The microstructure of the prepared ceramics was shown to be highly affected by the codoping. The grain size of the composition was decreased with the increase in Zn^{2+} concentration. The electrical studies showed that Zn^{2+} substitution at Cu^{2+} site resulted in enhancement in grain as well as grain boundary resistance, consequently IBLC effect is destroyed.

Gonzalez et al.[91] studied the influence of Sr and La replacing Ca and Cu, respectively, on the intrinsic properties of CCTO. The powders $Ca_{0.6}Sr_{0.4}Cu_3Ti_4O_{12}$, $CaCu_{2.85}La_{0.15}Ti_4O_{12}$, $Ca_{0.6}Sr_{0.4}Cu_{2.85}La_{0.15}Ti_4O_{12}$ and, pure $CaCu_3Ti_4O_{12}$ were prepared by mechanical alloying. The microstructure analyzed by SEM showed a smaller grain size for the co-doped CCTO (Figure 37).

They also reported that the co-doped CCTO-Sr La ceramic showed the smallest tan(δ) of 0.039 at 26.8 kHz compared to pure CCTO and single-doped ceramics. The co-doped sample reached a higher dielectric permittivity compared to the single-doped ceramics.

The effect of the codoping with Li^+ and Al^{3+} on the dielectric properties of CCTO was studied by Sun *et al.*[100] The codoped CCTO ceramics ($CaCu_{3-2x}Li_xAl_xTi_4O_{12}$, x = 0.05, 0.1, 0.15)

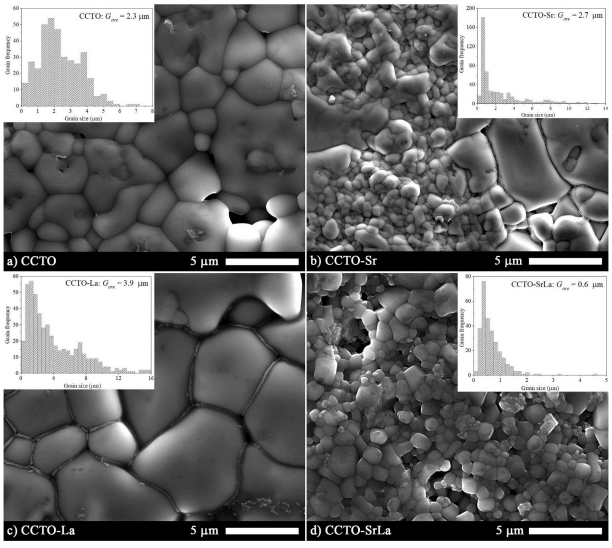

Figure 37. SEM micrographs of pure and doped CCTO: a) Pure CCTO, b) CCTO-Sr, c) CCTO-La, d) CCTO-Sr La. Insert plots: Grain size distribution for each sample. Riprented from (Gonzalez et al.). Copyright 2018 Elsevier.[91]

were prepared by a sol-gel method and were sintered at 1020–1080 °C for 8 h. The authors deduced that a very high dielectric constant of 1×10^5 with good dielectric-frequency as well as dielectric-temperature stability can be achieved in $CaCu_{2.8}Li_{0.1}Al_{0.1}Ti_4O_{12}$ ceramic sintered at 1060 °C. The average grain sizes, resistivity and the non-Ohmic properties are also improved compared to pure $CaCu_3Ti_4O_{12}$.

The effects of co-doping on dielectric and Electrical responses of $CaCu_3Ti_{4-x}(Nb_{1/2}In_{1/2})_x\ O_{12}$ Ceramics were studied by Boonlakhorn *et al.*[101] $CaCu_3Ti_{4-x}(Nb_{1/2}In_{1/2})_x\ O_{12}$ ceramics, where x = 0, 0.025, 0.05, 0.10, and 0.20, were prepared via a solid state reaction method. All the green bodies were sintered at 1090 °C for 18 h. The mean grain size of CCTO was decreased by doping with Nb^{5+} and In^{3+}. Surprisingly the authors observed an increase in tanδ with the increase of x. They explained this by the change of microstructure and grain resistance.

Rani *et al.*[102] prepared $Ca_{0.95}Nd_{0.05}Cu_3Ti_{4-x}Zr_xO_{12}$ (x = 0.01, 0.03 & 0.10) via solid method. SEM images demonstrated that grain size of the modified CCTO ceramics was controlled by Zr^{4+} ions due to solute drag effect. The mean grain size of the doped CCTO was decreased with the increase in subsequent concentrations of Zr^{4+} ions (Figure 38).

A huge value of dielectric permittivity ($\varepsilon_r \sim 16{,}902$) with nominal dielectric losses (tan δ ~ 0.067 at 1 kHz) was observed in a broad frequency range from 10^3 to 10^5 Hz for CCTO3 (x = 0.03) ceramic. Thus, it is concluded that the both dopant ions have played an independent role to improve the dielectric performance of CCTO system.

The same authors[103] focused on the Sr and Zn codoped CCTO. They prepared $Ca_{0.95}Sr_{0.05}Cu_3Ti_{4-x}Zn_xO_{12}$ (x = 0.01, 0.025, 0.05 & 0.10) powder by solid state method. They observed that the Zn ion has the same effect as the Zr ion and that grain size of the modified CCTO ceramics was controlled by Zn^{2+} ions due to solute drag effect. Dielectric parameters observed to be improved for higher Zn/Sr ratio in the studied compositions. The $Ca_{0.95}Sr_{0.05}Cu_3Ti_{3.9}Zn_{0.1}O_{12}$ ceramic composition shows a colossal dielectric permittivity of ~37,788 and loss ~0.049,

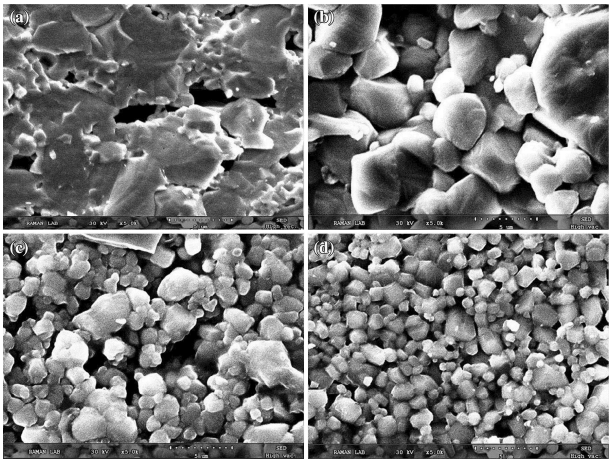

Figure 38. SEM images of fractured surfaces of a CCTO, b CCTO1, c CCTO2 and d CCTO3, ceramics. Reprinted by permission from (Nature/springer/ Journal of Materials science, Materials in Electronics) (Rani et al.) – *doi.org/10.1007/s10854-018-9150-9* Copyright (2018).[102]

which are stable within a broad frequency region. Reduced tanδ over a broad range of frequency was well ascribed to the highly insulating grain boundaries.

Guo *et al.*[104] showed that the co-doping of CCTO by Ni^{2+} and Zr^{4+} by sol gel method can affect the microstructure of the ceramics and their dielectric properties. The grain size increases with the increase in the dopant concentrations. The authors also mentioned that they obtained a very low tanδ of 0.026 for the $CaCu_{2.95}Ni_{0.05}Ti_{3.9}Zr_{0.1}O_{12}$ ceramic sintered at 1060 °C for 8 h with a very high ε′ value ~9.9×10^4 at about 9 kHz.

Du *et al.*[105] focused on the study of the codoping of CCTO by Y^{3+} on the A site and Al^{3+} on the B site in order to reduce the dielectric losses and simultaneously enhance the dielectric constants. Samples $Ca_{1-x}Y_xCu_3Ti_{4-x}Al_xO_{12}$ with different doping concentrations x = 0, 0.01, 0.02, 0.03, 0.05 and 0.07 have been prepared. No secondary phases were detected by XRD.

The dielectric properties showed that the dielectric losses of the doped ceramics are generally reduced and their dielectric constants are simultaneously enhanced across the frequency range up to 1 MHz. The doped sample with x = 0.05 exhibits the highest dielectric constant, which is well over 10^4 for frequency up to 1 MHz and is about 20% higher than the undoped sample.

Xu *et al.*[106] found that dielectric properties of CCTO were enhanced by its codoping with yttrium and zirconium. $CaCu_3Ti_{3.95}Zr_{0.0}O_{12}$ (CCTZO), $CaCu_3Ti_{3.97}Y_{0.03}O_{11.985}$ (CCTYO), and $CaCu_3Ti_{3.92}Y_{0.03}Zr_{0.05}O_{11.985}$ (CCTYZO) samples were prepared by citrate-nitrate combustion derived powders method. The SEM micrographs showed that Y_2O_3 and ZrO_2 additive can inhibit grain growth. The authors explained that the smaller grain sizes of Zr doped CCTO may be due to the slow diffusion of the larger Zr^{4+} ion substitutes of smaller Ti^{4+} ion, another possible explanation is that addition to larger Zr^{4+} ion, a high level of residual stress induced in the grain suppresses the grain growth of CCTO. Y doped CCTO also exhibits a smaller grain size, it may be due to the ability of Y^{3+} ion that suppresses the grain growth rate of CCTO ceramics, and rear-earth oxides could stop the grain boundaries from moving, which lead to fine grains.

A much better temperature and frequency stability of dielectric properties were realized in CCTYZO ceramics, and a low tan δ of 0.039 was observed at room temperature and 10 kHz for CCTYZO ceramics.

Dielectric properties of $Ca_{1-3x/2}Yb_xCu_{3-y}Mg_yTi_4O_{12}$ (x = 0.05, y = 0.05 and 0.30) prepared using a modified sol-gel method and sintered at 1070 °C for 4 h were investigated by Boonlakhorn *et al.*[107] They observed that Grain sizes of all co-doped samples were smaller than that of the un-doped CCTO sample. The authors concluded that the decrease in grain size of the co-doped CCTO ceramics was an important factor in reducing tanδ. Enhanced resistivity of each GB layer was due to Mg^{2+} doping.

Rhouma *et al.*[108] synthetized $Ca_{1-x}Sr_xCu_{3-y}Ni_yTi_4O_{12}$ for (x and y = 0 or 0.1), they found that Sr and Ni substitution leads to a ceramic densification and cubic grain form. They noticed that the dielectric permittivity increases (44,410) and the dielectric loss decreases (0.07) at low frequency of 1 kHz. In order to explain the grain growth, Raman spectra (Figure 39) measure-

ments were carried out for a good determination of grain and grain boundaries. The three main modes (447 cm^{-1}, 510 cm^{-1}, 576 cm^{-1}) appeared confirming the presence of CCTO at grains and grain boundaries, they found that CuO and TiO_2 exist as secondary phase on grain boundaries of the doped ceramics, which enhance the formation of liquid phase leading to grain boundary mobility and a grain growth.

To enhance dielectric properties of CCTO, lee *et al.*[109] suggested forming an electrical path for a contact network. Normally it is an artificial formation in which metallic materials used as micro capacitors to immigrate between thin dielectric layers in the ceramic materials. In CCTO ceramics a metastable phase is required for this electric path. As their previous study they noticed the formation of metastable phase after sintering at 1125 °C/2 h. This phase is formed when there is not enough energy to complete the sintering reaction. Usually silver or nickel are the representative migration material, lee *et al.* choose silver.[109] First they sintered CCTO at 1050 °C for 0.5, 2 and 12 h, metastable phase is formed in the 2 h sintered CCTO ceramics, and it is the liquid Cu phase. EDS analysis is used to approve the formation of metastable phase, by studying the stoichiometric report in different regions of the material. In order to study the effect of Ag migration into CCTO (Figure 40), after sintering a post heating at 700 °C/1 h was employed to Ag coated-CCTO. Dielectric studies applied on CCTO ceramics showed that the permittivity increases after post-heating to about 565.9×10^3 at 1 KHz.

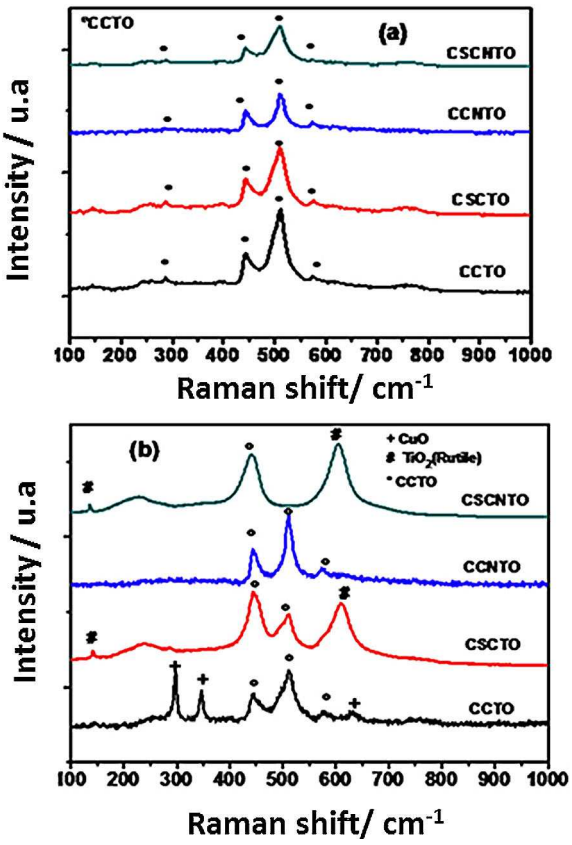

Figure 39. Raman Spectra (a) on grains and on grain boundaries (b). Reprinted from (Rhouma et al.). Copyright 2017 Elsevier.[108]

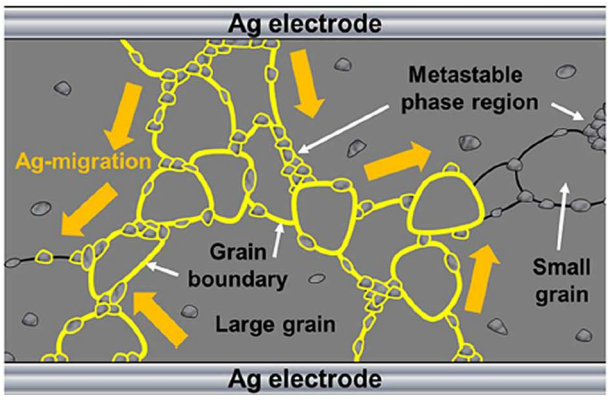

Figure 40. Schematic of the Ag-migration phenomenon into metastable phase including grain boundary for the 2 h sintered $CaCu_3Ti_4O_{12}$ ceramics. Reprinted from Springer Nature/ scientific reports (Lee et al). Copyright © 2018, Springer Nature.[109]

The effect of co-doping CCTO on microstructure, permittivity (ε_r) and loss tangent ($\tan\delta$) are resumed in Table 4. From these results, we can conclude that adding Yttrium to CCTO together with another dopant element can suppress the grain growth. Co-doping CCTO with Yttrium (Y) and Aluminum (Al) for instance yields a CCTO with a high dielectric constant ($2*10^4$) and a low dielectric loss ($\tan\delta = 0.048$).The results are explained by the following equation 3:

$$\varepsilon' = \varepsilon_{gb}\left(d/t\right) \quad (3)$$

Where (d) is the grain size and (t) is the grain boundary thickness. From SEM we see that grain size decreases after co-doping and grain boundaries are thinner so the ration (d/t) is high, which lead to a higher dielectric constant and a lower dielectric loss.

5. Applications

$CaCu_3Ti_4O_{12}$ showed exceptions dielectric properties useful for capacitors applications. Due to its outstanding structure where both atoms Ca^{2+} and Cu^{2+} with different ionic radius shared A site, CCTO can be used as well in photocatalytic application and especially in visible light. In addition CCTO is an antiferromagnetic compound; it is used to form composites with magnetic properties useful for antennas, GPS and other applications. In this section photocatalytic and magnetic properties will be reported.

5.1. Photocatalytic Properties

Accelerated industrial development and population growth forced science to find "green solutions" to solve problem of

pollutions, by using a renewable energy such as visible light. The decomposition reaction of pollutants and pharmaceutical waste occurs only upon UV lights, in which UV light shared 4% of wavelengths with visible light.[8,110] TiO_2 is acclaimed as a UV-light photocatalytic. To enhance TiO_2 performance in visible light, many approaches investigate the doping of TiO_2 with metal transitions.[111–113] While doping, a disordered structure could appear in TiO_2, limiting the efficiency of this approach. Perovskite structure ABO_3 has been investigated because A site is shared by two cations without causing a disordered lattice.[8] $CaCu_3Ti_4O_{12}$ perovskite showed a good photo-catalytic reaction against water pollutants and pharmaceutical waste.[8,109,110,114,115] As mentioned above, the specific structure of CCTO is the key of this function. It is related to photo-induced charge transition from ground state Cu^{2+},Ti^{4+} to excited state Cu^{3+},Ti^{3+} that CCTO have a visible light activity and they observed a direct band transition with a small band gap (1.52 eV).[8,110] CCTO was prepared using oxalate route to decompose pharmaceutical waste (erythrosin (dye), ciprofloxacin (antibiotic) and estriol (steroid)),[110] sol-gel and solid route to break-down water pollutants such as 4-chlorophenol.[8]

Kushwaha *et al.*[110] demonstrate that after 40 min of exposure a total decomposition of erythrosine dye (solution turned from pink to colorless). As shown in (Figure 41), the absorbance pic of erythrosine was observed at 525 nm and starts to decrease after exposure of the pink solution to the visible light irradiation in presence of CCTO pellets.

In 2017, *Hailili et al.*[115] used the molten salt method in order to synthetize $CaCu_3Ti_4O_{12}$. Five different salts were utilized to control the shape of crystals. By XRD, the formation of pure phase is confirmed for the five samples and no additional peaks for CuO or TiO_2 appear. It is well known that the presence of oxygen vacancy is very important for the photocatalytic behavior. For that, Electron Paramagnetic Resonance (EPR) measurements were carried out to investigate their presence in each sample. The measurements show that for all samples, the EPR signals are in the same position since all samples have the same Cu content. However samples with octahedron, nanorod and polyhedron shape samples have a large line width with high intensities in comparison with cubic shape samples indicating a high oxygen vacancy concentration. Photocatalytic test under visible irradiation are performed in the presence of tetracycline as pollutant. They deduced (Figure 42) that with

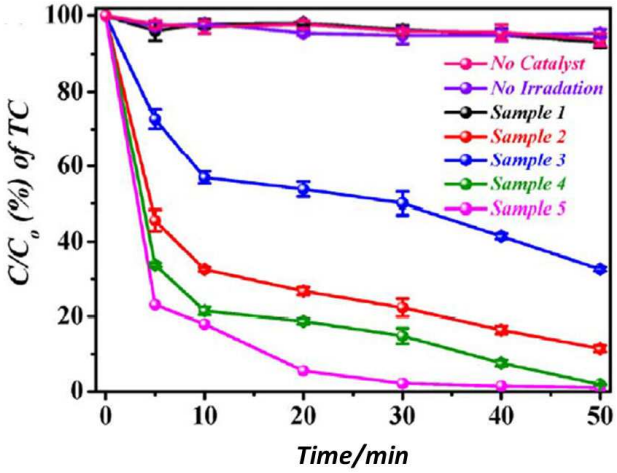

Figure 42. Degradation of TC in visible light irra-diation using different samples of $CaCu_3Ti_4O_{12}$. Copyright 2017 Elsevier.[115]

octahedron shape, the decomposition of TC achieved 99.1%, with higher constant $k = 1.1*10^{-1}$ min^{-1} (first low of kinetics). These results are explained by 2 reasons: (i) the defects that enhance the active sites and (ii) an effective separation of electron-hole pairs to produce high efficiency in photocatalytic activity.

In order to enhance pollutant decomposition under visible light, *Hailili et al.*[116] synthesized a single crystal of $CaCu_3Ti_4O_{12}$ octahedron by molten salt. This crystal contains oxygen vacancies, metal deficiencies of Cu^+ and Ti^{3+} and coexposed facets of ({001},{111}).

In CCTO (perovskite type ABO_3), Ca and Cu atoms share the same A site and Cu is bonded to O atom (CuO_4) and to TiO_6 octahedron with one O atom, to form TiO6 and CuO_4 cluster. So any distortion of cluster or Ti displacement in TiO_6 causes a defect in the crystallite structure of CCTO and results in an imperfection. The defect was confirmed in EPR measurement by the presence of the characteristic pic of Ti^{3+} ($3d^1$) and Cu^+ at g value of 1.982 and 2.077 respectively which cause a distortion for Ti–O–Ti bond and generate TiO_5 distorted square structure formed from Ti^{3+} and Ti^{4+} and defects in CuO_4 planar. To characterize the heterojunctions facets, they calculate the band energy and density of states (DSO) of {001} and {111} surfaces by DFT. They deduced that there is a difference in level energy between conduction band (CB) and valence band (VB) levels of the exposed {001} and {111} facets; so facets heterojunctions can be formed. Under visible light irradiation, photoinduced

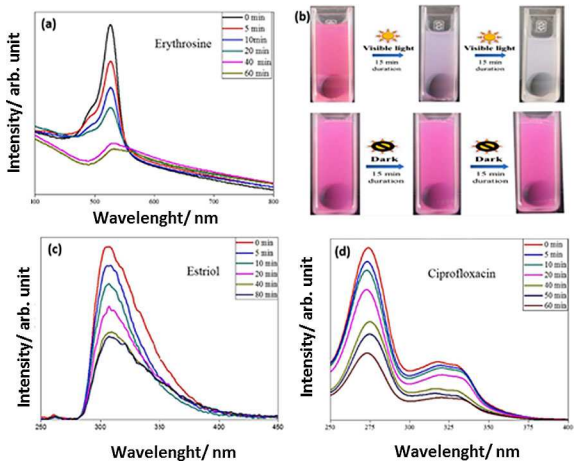

Figure 41. (a) Change in absorbance of Erythrosine (525 nm) (b) Color change in erythrosine under dark and light (Figure drawn by author H.S. Kushwaha) (c) Change in absorbance of Ciprofloxacin (276 nm) and (d) fluorescence emission of estriol (305 nm excited at 240 nm) with time in photocatalytic degradation using CCTO pellets under visible light ($\lambda > 420$ nm). Reprinted from (Kushwaka et al). Copyright 2016 Creative Commons.[110]

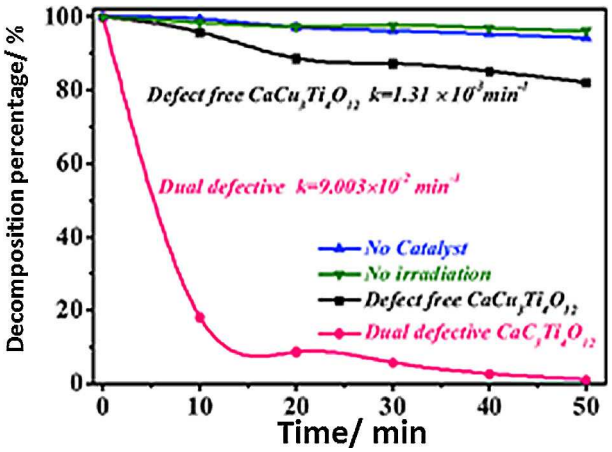

Figure 43. Comparison visible light degradation ratio and corresponding apparent rate constants (k) of tetracycline in the presence of octahedron shaped dual defective and defect free $CaCu_3Ti_4O_{12}$. Reprinted fom (Haillili et al.). Copyright 2019 IEEE.[116]

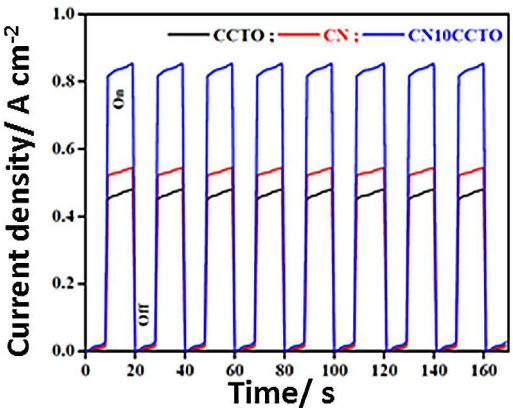

Figure 44. Current density vs. time plot of CCTO, CN and CN10CCTO (10 wt% CN in CCTO). Reprinted from (Pal et al.). Copyright 2019 IEEE.[118]

electrons migrate from {001} to the exposed facets of {111} preferred as reduction sites because the electrons accumulation and {001} facets served as oxidation sites since photoinduced holes are accumulated on it. Figure 43 showed the degradation of tetracycline under visible light in presence of CCTO with and without defect. They deduced that 99.34% from tetracycline is decomposed in the presence of defect dual CCTO with large normalized rate constant of $1.06*10^{-2}$ min^{-1}.

Zhu et al.[117] tested the photo-assisted fenton-like process based on sulfate radicals using $CaCu_3Ti_4O_{12}$ as catalyst to remove pharmaceutical pollutants (ibuprofen) from water. Fenton-like process is based on sulfate radicals ($SO_4^{\bullet-}$), in which sulfate radicals with higher oxidative potential (2.5–3.1 V) exhibit a higher oxidation power compared with hydroxyl radicals. Furthermore ($SO_4^{\bullet-}$) has a long life time (30–40 μs) and a large range of working pH (2–9). They used molten salt synthesis to produce different shapes of CCTO catalyst by modifying sintering times. Cubic structures are formed at 775 °C sintered for 6 h (sample CCTO-6) and fibers are produced at 775 °C sintered for 14 h (sample CCTO-14). Photocatalytic behavior is tested for different systems, the ternary one (visible light/ $CaCu_3Ti_4O_{12}$ (sample-14)/peroxymonosulfate) promotes ibuprofen's removal to 91.8% in 30 min. CCTO-14 showed oxygen vacancies and production of Cu^+ since Cu^{2+} intensity decreases as shown in EPR measurement. It is related to the fact that under visible light, photogenerated-electrons are free to move into the crystallographic lattice and allow reducing Cu^{2+} to Cu^+, thus make enable peroxymonosulfate to generate sulfate radicals and reduce the rate of electron-holes recombination.

Pal et al.[118] synthesis $CaCu_3Ti_4O_{12}$-Carbon nitride composites as catalyst using low temperature thermal treatment (~150 °C). They investigate the decomposition of methylene blue in the presence of H_2O_2 activator, in the presence of LED light irradiation and the catalyst. They noticed that for 10 wt% CN in CCTO (sample: CN10CCTO), the decomposition of dye achieved 96% in 1 h. Optical properties confirms charge transition from Cu^{2+}, Ti^{4+} ground states to Cu^{3+}, Ti^{3+} excited states respectively. From transient photocurrent study (Figure 44), they showed that CN10CCTO has the highest photocurrent value, which is attributing to the efficacy of charge separation of the charge carriers leading to an enhanced photocatalytic activity.

5.2. Magnetic Properties

A need to developed magnetic materials was the aim of researches in the 20th century. The best application is showed for materials where their coercivity and magnetization are optimized. Practical progress in magnetism largely depends on ferromagnetic materials, in which the mastery of coercivity was resulted from combined control of magnetocrystalline anisotropy and microstructure.[119] Ferromagnetic materials had a large range of magnetic dipoles that can be switched by applying a determined magnetic field.[120] The challenge is to correlate nanostructure properties and magnetic properties, and in order to explain this correlation, nanostructure materials were classified into different categories. Bulk materials or type D is one of this nanostructure materials, it is formed from grains and interfaces. With type D, the magnetic behavior cannot be predicted by applying theories for polycrystalline at nanoscales, because it is depending from grain boundaries and interaction.[121]

$CaCu_3Ti_4O_{12}$ is a bulk material with a antiferromagnetic behavior below Neel temperature ($T_N = 25$ K) studied with neutron diffraction and susceptibility measurements,[122] due to spins ($S = 1/2$) aligned antiferromagnetically on the A sites Cu^{2+} [56] In order to enhance CCTO magnetic properties and to produce multiferroic material stable at room temperature, many investigations were performed by doping CCTO.[56,122,123]

Wang et al.[58] doped CCTO ceramics using Cobalt (Co) by solid-state method. They showed from hysteresis loops, a weak ferromagnetism due to the superexchange interaction along Cu-O-Co-O-Cu path attributed to the small amount of Co substitution for the Ti site, instead of antiferromagnetic superexchange via Cu-O-Ti-O-Cu path.

Pansara *et al.*[123] synthesize $CaCu_{3-x}Ti_{4-x}Fe_{2x}O_{12}$ (x = 0.0–07) using solid state reaction. From M-H loops, they conclude that the material for x = 0.0–0.3 presents an antiferromagnetic behavior while x = 0.5 and 0.7 present ferromagnetic properties. To explain the influence of Fe doping on CCTO, ^{27}Fe Mossbauer spectroscopy is used to investigate the oxidation number of Fe doped into the crystallite lattice. They conclude from hyperfine interaction parameters such as isomer shift (IS), Quadruple splitting (QS) and magnetic hyperfine field (HF) that Fe is in Fe^{3+} form in which for x = 0.5 and 0.7 Fe^{3+} ions prefer A′-site. Fe^{3+} in A′-site changes the superexchange interaction by increasing the Cu-Cu distance and increase the ferromagnetism by the dominant superexchange interaction through Cu(Fe)-O-Ti(Fe)-O-Cu(Fe) path.

Raval *et al.*[124] investigate the effect of ball milling, microwave assisted heating and rapid thermal cooling on magnetic properties in polycrystalline $CaCu_3Ti_4O_{12}$. Ball-milling induce curtails hybridization of empty Ti-3d orbitals with Cu-3d and O-2p orbitals and secondary phase formation. M-T curves show pure antiferromagnetic peak for unmilled sample in which Cu–Cu bond distance is 3.6963 Å, and a weak ferromagnetic peak for 16 h milling in which Cu–Cu bond is longest.

Gavrilova et al.[125] synthesized a CCTO based nanocomposite $(SrFe_{12}O_9)_x(CaCu_3Ti_4O_{12})_{1-x}$ (x = 0.01, 0.03, 0.07, 0.1) using solid state method. Electron spin resonance (EPS) showed two different lineshapes between x = 0.03–0.07 group and x = 0.01–0.1 group. For x = 0.01, two lines appear, one is due to Cu^{2+} paramagnetic signal and the second is related to ferromagnetic signal from $CaCu_3Ti_{4-y}Fe_yO_{12}$ solid solution. The position of ferromagnetic line shifts to g = 2 (H = 3300 Oe) while increasing the temperature. For x = 0.03 and 0.07, TEM analysis confirmed the formation of nanostructured composites where SFO inclusions are inside the matrix. These results confirm the presence of two lines by EPS, in which one is attributed to the paramagnetic behavior of CCTO and second is a ferromagnetic line from SFO component. The EPS spectra for x = 0.03 and 0.07 become less symmetric with increasing temperature.

6. Conclusion and Outlook

Recent investigations focus on high dielectric material especially ceramics to energy storage and environmental application. Ceramics with specific dielectric properties are highly demanded because of their fast charge-discharge comparing with batteries. CCTO-perovkite is a ceramic founded in 2000, with high permittivity stable at a large range of frequencies and temperatures. In this review, an overview on the history of CCTO ceramics, the different manufacturing methods (synthesis and sintering) and the different elements used as dopant for CCTO is given. The effect of all these parameters on the microstructure and dielectric properties is discussed. The origin of high dielectric constant in CCTO ceramics is not fully understood. Many hypotheses were deducted from different studies. Intrinsic hypotheses is based on that high dielectric constant is the result of TiO_6 titled octahedral planar. By impedance spectroscopy, it was discovered that CCTO ceramics are heterogeneous, composed of semiconducting grains and insulating grain boundaries (IBLC model). Third hypothesis explain that this high dielectric constant comes from the interfacial reactions between electrodes used and the surface of the material. IBLC model is the most accepted due to that dielectric loss can be controlled with controlling grain boundaries, which allow CCTO to be useful in electronic applications. Studies focused on decreasing loss tangent with maintaining a high dielectric constant stable at large range of frequencies are summarized.

Different synthesis methods were used for the synthesis of CCTO: Solid state route, wet chemistry method at room temperature and normal pressure (sol-gel and coprecipitation), hydrothermal method (under high pressure), microwave and autocombustion methods. It is been observed that the dielectric properties highly depend on the synthesis technique. The best dielectric properties were shown by the ceramics prepared via the solid state route despite the high temperature used. Using wet chemistry method is a better approach to obtain a homogeneous and controlled microstructure. New trend in this area should be in the direction of finding new synthesis methods such as molten salt shielded synthesis able to give a homogenous micro or nanostructures. Such techniques could help to reduce the synthesis temperature and achieve high permittivity and low loss tangent.

The use of different sintering techniques leads to different dielectric properties. Conventional sintering and spark plasma are one-step approaches for the formation of CCTO ceramics, contrariwise to microwave sintering and thermobaric treatment that need a pre-conventional sintering step. Discovering new sintering method using less energy is necessary for industrial applications of CCTO such a cold pressing sintering applied in ceramic field.

To enhance dielectric properties and maintain a high dielectric permittivity with a low dielectric loss, doping CCTO was one of the aims of researchers. Many atoms with different valence are chosen to be inserted into the crystalline structure in order to change the charge distribution of elements. From results showed in this review, it is clear that these elements have significant influence on dielectric properties and even on grain morphologies and boundaries. An optimal dopant could be inserted into the lattice without making distortion, but should suppress the grain growth in order to improve the dielectric properties. Till now, a huge variety of element was used as dopant for CCTO.

Because of its specific structure, several studies focused on photocatalytic function of CCTO and especially in the range of visible light for environmental issues. Pure CCTO showed an important photocatalytic performance in presence of pharmaceutical and water pollutants in visible light. CCTO showed as well an antiferromagnetic behavior based on neutron diffraction; several studies were performed in order to form multiferroic compounds, such as doping CCTO by different ferroelectric elements (Fe, Nb, Co).

Despite his colossal dielectric properties, and to the best of our knowledge, CCTO is not used in industrial applications. In order to bring CCTO based devices on the market, more

investigations should be performed in order to tune their properties for wide range of applications such as capacitor, varistor, GPS devices, and antennas as well as as photo-electrocatalytic materials able to degrades pharmaceutical and dye pollutants.

Conflict of Interest

The authors declare no conflict of interest.

Keywords: ferroelectric materials · magnetic properties · perovskites · photocatalytic properties · copper calcium titanate

[1] Y. XU, Ferroelectric Materials and their applications 1st Edition BooK.**1991**.
[2] C. J. Howard, H. T. Stokes, *Acta Crystallogr. Sect. B.* **1998**, *54*, 782–789.
[3] V. M. Goldschmidt – Akad, Oslo, *I. Mat-Nat. K1*, **1926**.
[4] W. Forrester, R. Hinde, *Nature.* **1945**, *156*, 177.
[5] N. Banerjee, S. Krupanidhi, **2010**, *2*, 688–693.
[6] M. A. Subramanian, D. Li, N. Duan, B. Reisner, A. Sleight, *J. Solid State Chem.* **2000**, *151*, 323–325.
[7] D. C. Sinclair, T. B. Adams, F. Morrison, A. R. West, *Appl. Phys. Lett.* **2002**, *80*, 2153–2155.
[8] J. Clark, M. Dyer, R. Palgrave, C. Ireland, J. Darwent, J. Claridge, M. Rosseinsky, *J. Am. Chem. Soc.* **2011**, *133*, 1016–1032.
[9] L. Sun, R. Zhang, Z. Wang, E. Cao, Y. Zhang, L. Ju, *RSC Adv.* **2016**, *6*, 55984–55989.
[10] W. Li, L. Tang, F. Xue, Z. Xin, Z. Luo, G. Du, *Ceram. Int.* **2017**, *43*, 6618–6621.
[11] A. Smith, T. Calvarese, A. Sleight, M. Subramanian, *J. Solid State Chem.* **2009**, *182*, 409–411.
[12] M. Cohen, J. Neaton, L. He, D. Vanderbilt, *J. Appl. Phys.* **2003**, *94*, 3299–3306.
[13] M. Li, D. C. Sinclair, A. R. West, *J. Appl. Phys.* **2011**, *109*, 084106.
[14] M. Li, Z. Shen, M. Nygren, A. Feteira, D. C. Sinclair, A. R. West, *J. Appl. Phys.* **2009**, *106*, 104106.
[15] T. B. Adams, D. C. Sinclair, A. R. West, *Phys. Rev. B.* **2006**, *73*, 94124.
[16] R. K. Pandey, W. A. Stapleton, J. Tate, A. K. Bandyopadhyay, I. Sutanto, S. Sprissler, S. Lin, *AIP Adv.* **2013**, *3*, 62126.
[17] H. Ghayour, M. Abdellahi, *Powder Technol.* **2016**, *292*, 84–93.
[18] H. S. Bhatti, S. T. Hussain, F. A. Khan, S. Hussain, *Appl. Surf. Sci.* **2016**, *367*, 291–306.
[19] M. Ahmadipour, M. F. Ain, Z. A. Ahmad, *Nano-Micro Lett.* **2016**, *8*, 291–311.
[20] G. J. Lee, E. K. Park, S. A. Yang, J. J. Park, S. D. Bu, M. K. Lee, *Sci. Rep.* **2017**, *7*, 46241.
[21] H. Yu, H. Liu, H. Hao, L. Guo, C. Jin, Z. Yu, M. Cao, *Appl. Phys. Lett.* **2007**, *91*, 222911.
[22] P. Thongbai, J. Jumpatam, B. Putasaeng, T. Yamwong, S. Maensiri, *J. Appl. Phys.* **2012**, *112*, 114115.
[23] T. T. Fang, H. Y. Chung, S. C. Liou, *J. Appl. Phys.* **2009**, *106*, 54106.
[24] N. Tripathy, K. C. Das, S. P. Ghosh, G. Bose, J. P. Kar, *Mater. Sci. Eng.* **2016**, *115*, 12022.
[25] B. G. Rao, D. Mukherjee, B. M. Reddy, *Nanostruct. Novel Ther.* **2017**, 1–36.
[26] P. Mao, J. Wang, S. Liu, L. Zhang, Y. Zhao, L. He, *J. Alloys Compd.* **2019**, *778*, 625–632.
[27] B. Zhu, Z. Wang, Y. Zhang, Z. Yu, J. Shi, R. Xiong, *Mater. Chem. Phys.* **2009**, *113*, 746–748.
[28] R. Kumar, M. Zulfequar, L. Sharma, V. N. Singh, T. D. Senguttuvan, *Cryst. Growth Des.* **2015**, *15*, 1374–1379.
[29] S. Patra, ethesis.nitrkl.ac.in.2009.
[30] A. Lopera, M. A. Ramirez, C. García, C. Paucar, J. Marín, *Inorg. Chem. Commun.* **2014**, *40*, 5–7.
[31] C. Masingboon, S. Rungruang, *J. Phys. Conf. Ser.* **2017**, *901*, 012101.
[32] R. M. German, *Sintering: From Empirical Observations to Scientific Principles* **2014**, 1–12.
[33] L. Jaworska, J. Cyboroń, S. Cygan, J. Laszkiewicz-Łukasik, M. Podsiadło, P. Novak, Y. Holovenko, *Mater. Sci. Eng.* **2018**, *329*, 012004.
[34] M. Oghbae, O. Mirzaee, *J. Alloys Compd.* **2010**, *494*, 175–189.
[35] B. Barbier, C. Combettes, S. Guillemet-Fritsch, T. Chartier, F. Rossignol, A. Rumeau, T. Lebey, E. Dutarde, *J. Eur. Ceram. Soc.* **2009**, *29*, 731–735.
[36] S. Krohns, P. Lunkenheimer, S. G. Ebbinghaus, A. Loidl, *J. Appl. Phys.* **2008**, *103*, 084107.
[37] M. C. Ferrarelli, D. C. Sinclair, A. R. West, H. A. Dabkowska, A. Dabkowski, G. M. Luke, *J. Mater. Chem.* **2009**, *19*, 5916–5919.
[38] P. Fiorenza, V. Raineri, S. G. Ebbinghaus, R. Lo-Nigro, *CrystEngComm.* **2011**, *13*, 3900–3904.
[39] R. Schmidt, S. Pandey, P. Fiorenza, D. C. Sinclair, *RSC Adv.* **2013**, *3*, 14580–14589.
[40] A. O. Turky, M. M. Rashad, Z. I. Zaki, I. A. Ibrahim, M. Bechelany, *RSC Adv.* **2015**, *5*, 18767–18772.
[41] S. Y. Chung, I. D. Kim, S. JL. Kang, *Nat. Mater.* **2004**, *3*, 774–778.
[42] R. R. Mishra, A. K. Sharma, *Composites Part A.* **2016**, *81*, 78–97.
[43] R. Kumar, M. Zulfequar, T. D. Senguttuvan, *J. Electroceram.* **2019**, *42*, 41–46.
[44] X. Ouyang, P. Cao, S. Huang, W. Zhang, Z. Huang, W. Gao, *J. Electron. Mater.* **2015**, *44*, 2243–2249.
[45] P. Y. Raval, A. R. Makadiya, P. R. Pansara, P. U. Sharma, N. H. Vasoya, J. A. Bhalodia, S. Kumar, S. N. Dolia, K. B. Modi, *Mater. Chem. Phys.* **2018**, *212*, 343–350.
[46] O. Guillon, J. Gonzalez-Julian, B. Dargatz, T. Kessel, G. Schierning, J. Räthel, M. Herrmann, *Adv. Eng. Mater.* **2014**, *16*, 830–849.
[47] R. Kumar, M. Zulfequar, T. D. Senguttuvan, *J. Mater. Sci. Mater. Electron.* **2015**, *26*, 6718–6722.
[48] R. Kumar, M. Zulfequar, T. D. Senguttuvan, *J. Mater. Sci. Mater. Electron.* **2016**, *27*, 5233–5237.
[49] L. Ni, M. Fu, X. Ren, Y. Zhang, *J. Mater. Sci. Mater. Electron.* **2017**, *28*, 10191–10198.
[50] H. Lin, X. He, Y. Gong, D. Pang, Z. Yi, *Ceram. Int.* **2018**, *44*, 8650–8655.
[51] S. Zhai, E. Ito, *Geosci. Front.* **2011**, *2*, 101–106.
[52] L. F. Xu, C. Mao, V. V. Marchenkov, K. Sun, T. V. Dyachkova, A. P. Tyutyunnik, Y. G. Zainulin, C. P. Yang, S. H. Liang, *Phys. Lett. A* **2018**, *382*, 2861–2867.
[53] C. Mao, L. Xu, V. V. Marchenkov, T. V. Dyachkova, A. P. Tyutyunnik, Y. G. Zainulin, C. Yang, *Ceram. Int.* **2018**, *44*, 20069–20074.
[54] J. W. Lee, J. H. Koh, *Ceram. Int.* **2017**, *43*, 9493–9497.
[55] L. F. Xu, K. Sun, X. Feng, H. B. Xiao, R. L. Wang, C. P. Yang, *Int. J. Mod. Phys. B.* **2017**, *31*, 1750133.
[56] C. Mu, Y. Song, H. Wang, X. Wang, *J. Appl. Phys.* **2015**, *117*, 17B723.
[57] Z. Kafi, A. Kompany, H. Arabi, Z. A. Khorsand, *J. Alloys Compd.* **2017**, *727*, 168–176.
[58] J. Wang, Z. Lu, T. Deng, C. Zhong, Z. Chen, *J. Eur. Ceram. Soc.* **2018**, *38*, 3505–3511.
[59] E. Swatsitang, T. Putjuso, *J. Eur. Ceram. Soc.* **2018**, *38*, 4994–5001.
[60] A. Sakthisabarimoorthi, S. A. Martin Britto Dhas, R. Robert, M. Jose, *Mater. Res. Bull.* **2018**, *106*, 81–92.
[61] M. Li, Q. Liu, C. X. Li, *J. Alloys Compd.* **2017**, *699*, 278–282.
[62] J. Jumpatam, B. Putasaeng, N. Chanlek, P. Kidkhunthod, P. Thongbai, S. Maensiri, P. Chindaprasirt, *RSC Adv.* **2017**, *7*, 4092–4101.
[63] R. Late, H. M. Rai, S. K. Saxena, R. Kumar, A. Sagdeo, P. R. Sagdeo, *J. Mater. Sci. Mater. Electron.* **2016**, *27*, 5878–5885.
[64] Z. Wang, J. Guo, W. Hao, E. Cao, Y. Zhang, L. Sun, P. Xu, *J. Electroceram.* **2018**, *40*, 115–121.
[65] J. Chen, T. Li, H. Y. Dai, Z. P. Chen, *Diffus. Defect Data, Pt. A* **2017**, *373*, 241–244.
[66] A. Srivastava, *Am. J. Mater. Synth. Process.* **2018**, *2*, 90–93.
[67] X. Huang, H. Zhang, J. Li, Y. Lai, *J. Mater. Sci. Mater. Electron.* **2016**, *27*, 11241–11247.
[68] L. Sun, R. Zhang, Z. Wang, E. Cao, Y. Zhang, L. Ju, *J. Alloys Compd.* **2016**, *663*, 345–350.
[69] E. Swatsitang, K. Prompa, T. Putjuso, *J. Mater. Sci. Mater. Electron.* **2018**, *29*, 12639–12651.
[70] C. Wang, W. Ni, D. Zhang, X. Sun, J. Wang, H. Li, N. Zhang, *J. Electroceram.* **2016**, *36*, 46–57.
[71] S. S. Kouassi, J. P. Sagou, C. Autret-Lambert, S. Dridy, M. Lethiecq, *Adv. Mater.* **2017**, *6*, 57–65.
[72] S. Senda, S. Rhouma, E. Torkani, A. Megriche, C. Autret, *J. Alloys Compd.* **2017**, *698*, 152–158.
[73] J. Wang, Z. Lu, T. Deng, C. Zhong, Z. Chen, *J. Am. Ceram. Soc.* **2017**, *100*, 4021–4032.

[74] J. Boonlakhorn, B. Putasaeng, P. Thongbai, *Ceram. Int.* **2019**, *45*, 6944–6949.
[75] W. Li, T. Zhang, S. Liu, Z. Lu, R. Xiong, *Ceram. Int.* **2017**, *43*, 4366–4371.
[76] J. A. Cortés, G. Cotrim, S. Orrego, A. Z. Simões, M. A. Ramírez, *J. Alloys Compd.* **2018**, *735*, 140–149.
[77] M. Sahu, S. Hajra, R. N. P. Choudhary, *SN Appl. Sci.* **2018**, *1*, 13.
[78] S. Amhil, E. Choukri, S. Ben Moumen, A. Bourial, L. Essaleh, *Phys. B* **2019**, *556*, 36–41.
[79] L. Singh, B. C. Sin, I. W. Kim, K. D. Mandal, H. Chung, Y. Lee, *J. Am. Ceram. Soc.* **2016**, *99*, 27–34.
[80] S. S. Kouassi, J. P. Sagou, C. Autret-Lambert, S. Dridy, A. Nautiyal, M. Lethiecq, *Int. J. Mater. Sci. Appl.* **2017**, *6*, 54–64.
[81] L. Tang, F. Xue, P. Guo, Z. Xin, Z. Luo, W. Li, *Ceram. Int.* **2018**, *44*, 18535–18540.
[82] R. Xue, G. Zhao, J. Chen, Z. Chen, D. Liu, *Mater. Res. Bull.* **2016**, *76*, 124–132.
[83] R. Espinoza-González, E. Mosquera, *Ceram. Int.* **2017**, *43*, 14659–14665.
[84] D. Xu, Y. Zhu, B. Zhang, X. Yue, L. Jiao, J. Song, S. Zhong, J. Ma, L. Bao, L. Zhang, *J. Mater. Sci. Mater. Electron.* **2018**, *29*, 5116–5123.
[85] S. Senda, S. Rhouma, E. Torkani, A. Megriche, C. Autret, *J. Alloys Compd.* **2017**, *698*, 152–158.
[86] X. Huang, H. Zhang, M. Wei, Y. Lai, J. Li, *J. Alloys Compd.* **2017**, *708*, 1026–1032.
[87] W. Makcharoen, W. Punsawat, *Mater. Today* **2017**, *4*, 6234–6238.
[88] J. Boonlakhorn, B. Putasaeng, P. Kidkhunthod, P. Thongbai, *Mater. Des.* **2016**, *92*, 494–498.
[89] J. Boonlakhorn, P. Kidkhunthod, N. Chanlek, P. Thongbai, *J. Eur. Ceram. Soc.* **2018**, *38*, 137–143.
[90] J. Deng, X. Sun, S. Liu, L. Liu, T. Yan, L. Fang, B. Elouadi, *J. Adv. Dielectr.* **2016**, *06*, 1650009.
[91] R. Espinoza-González, S. Hevia, Á. Adrian, *Ceram. Int.* **2018**, *44*, 15588–15595.
[92] T. C. Porfirio, E. N. S. Muccillo, *Ceram. Int.* **2016**, *42*, 12005–12009.
[93] J. Boonlakhorn, P. Thongbai, B. Putasaeng, T. Yamwong, S. Maensiri, *J. Alloys Compd.* **2014**, *612*, 103–109.
[94] H. Katayama-Yoshida, T. Nishimatsu, T. Yamamoto, N. Orita, *J. Phys. Condens. Matter* **2001**, *13*, 8901–8914.
[95] A. Wen, D. Yuan, X. Zhu, J. Zhu, D. Xiao, J. Zhu, *Ferroelectrics* **2016**, *492*, 1–9.
[96] J. Boonlakhorn, P. Thongbai, *Ceram. Int.* **2017**, *43*, 12736–12741.
[97] L. Ren, L. Yang, C. Xu, X. Zhao, R. Liao, *J. Alloys Compd.* **2018**, *768*, 652–658.
[98] L. Bai, Y. Wu, L. Zhang, *J. Alloys Compd.* **2016**, *661*, 6–13.
[99] S. Rani, N. Ahlawat, R. Punia, K. M. Sangwan, P. Khandelwal, *Ceram. Int.* **2018**, *44*, 23125–23136.
[100] L. Sun, Q. Ni, J. Guo, E. Cao, W. Hao, Y. Zhang, L. Ju, *Appl. Phys. A* **2018**, *124*, 428.
[101] J. Boonlakhorn, P. Kidkhunthod, P. Thongbai, *J. Phys. Conf. Ser.* **2017**, *901*, 12078.
[102] S. Rani, N. Ahlawat, K. M. Sangwan, S. Rani, R. Punia, J. Malik, *J. Mater. Sci. Mater. Electron.* **2018**, *29*, 10825–10833.
[103] S. Rani, N. Ahlawat, K. M. Sangwan, R. Punia, A. Kumar, *J. Alloys Compd.* **2018**, *769*, 1102–1112.
[104] J. Guo, L. Sun, Q. Ni, E. Cao, W. Hao, Y. Zhang, Y. Tian, L. Ju, *Appl. Phys. A* **2018**, *124*, 635.
[105] G. Du, F. Wei, W. Li, N. Chen, *J. Eur. Ceram. Soc.* **2017**, *37*, 4653–4659.
[106] Z. Xu, H. Qiang, Y. Chen, Z. Chen, *Mater. Chem. Phys.* **2017**, *191*, 1–5.
[107] J. Boonlakhorn, P. Kidkhunthod, P. Thongbai, S. Maensiri, *Ceram. Int.* **2016**, *42*, 8467–8472.
[108] S. Rhouma, S. Saîd, C. Autret, D. Almeida, S. Didry, M. El Amrani, A. Megriche, *J. Alloys Compd.* **2017**, *717*, 121–126.
[109] J. W. Lee, G. H. Lee, D. J. Shin, J. Kim, S. J. Jeong, J. H. Koh, *Sci. Rep.* **2018**, *8*, 1392.
[110] H. S. Kushwaha, N. A. Madhar, B. Ilahi, P. Thomas, A. Halder, R. Vaish, *Sci. Rep.* **2016**, *6*, 18557.
[111] M. Nasr, S. Balme, C. Eid, R. Habchi, P. Miele, M. Bechelany, *J. Phys. Chem. C* **2017**, *121*, 261–269.
[112] M. Nasr, C. Eid, R. Habchi, P. Miele, M. Bechelany, *ChemSusChem* **2018**, *11*, 3023–3047.
[113] M. Nasr, R. Viter, C. Eid, R. Habchi, P. Miele, M. Bechelany, *New J. Chem.* **2017**, *41*, 81–89.
[114] A. Sen, K. K. Chattopadhyay, *J. Mater. Sci. Mater. Electron.* **2016**, *27*, 10393–10398.
[115] R. Hailili, Z. Q. Wang, Y. Li, Y. Wang, V. K. Sharma, X. Q. Gong, C. Wang, *Appl. Catal. B* **2018**, *221*, 422–432.
[116] R. Hailili, Z. Q. Wang, X. Q. Gong, C. Wang, *Appl. Catal. B* **2019**, *254*, 86–97.
[117] Y. Zhu, T. Wang, W. Wang, S. Chen, E. Lichtfouse, C. Cheng, J. Zhao, Y. Li, C. Wang, *Environ. Chem. Lett.* **2019**, *17*, 481–486.
[118] K. Pal, A. Mondal, R. Jana, P. P. Ray, A. Gayen, *Appl. Surf. Sci.* **2019**, *467–468*, 543–553.
[119] J. M. D. Coey, *J. Alloys Compd.* **2001**, *326*, 2–6.
[120] P. Mandal, M. J. Pitcher, J. Alaria, H. Niu, P. Borisov, P. Stamenov, J. B. Claridge, M. J. Rosseinsk, *Nature* **2015**, *525*, 363.
[121] D. L. Leslie-Pelecky, R. D. Rieke, *Chem. Mater.* **1996**, *8*, 1770–1783.
[122] A. Koitzsch, G. Blumberg, A. Gozar, B. Dennis, A. P. Ramirez, S. Trebst, S. Wakimoto, *Phys. Rev. B* **2002**, *65*, 052406.
[123] P. R. Pansara, P. Y. Raval, N. H. Vasoya, S. N. Dolia, K. B. Modi, *Phys. Chem. Chem. Phys.* **2018**, *20*, 1914–1922.
[124] P. Y. Raval, P. R. Pansara, A. R. Makadiya, N. H. Vasoya, S. N. Dolia, K. B. Modi, *Ceram. Int.* **2018**, *44*, 17667–17674.
[125] T. P. Gavrilova, J. A. Deeva, I. V. Yatsyk, A. R. Yagfarova, I. F. Gilmutdinov, N. M. Lyadov, F. O. Milovich, T. I. Chupakhina, R. M. Eremina, *Phys. B* **2018**, *536*, 303–309.

Manuscript received: April 15, 2019
Revised manuscript received: June 8, 2019